UWB localization system for partially GPS-denied robotic applications

POLITECNICO
DI TORINO

Giovanni Fantin

Supervisor: Prof. Marcello Chiaberge

Collegio di Ingegneria Informatica, del Cinema e Meccatronica
Politecnico di Torino

MSc in Mechatronic Engineering

April 2019

Abstract

Most common robotic outdoor navigation systems typically rely upon global positioning system, nevertheless there are several scenarios in which the GPS alone is not enough. The presence of tall buildings, trees or other obstacles can cause a substantial deterioration of the position estimation of the robot due to blockage of line-of-sight and multipath effects. So, dealing with partially GPS-denied environments makes it necessary to develop ad hoc solutions to aid navigation.

This work moves the first steps towards the development of a localization system based on drones and ultra-wide band technologies. The idea is to use three or four drones hovering above the working area of the rover where they can be localized using GPS. Moreover, both the UAVs and the ground vehicle are equipped with ultra-wide band sensors in order to precisely measure the relative distance between all the agents. With this information, it is possible to compute the position of the UGV using trilateration algorithms.

The first part of this thesis consists in a description and classification of the most common localization systems based on radio signals; these technologies have been developed for general purposes but most of them can be applied to robotic navigation. Moreover, the functioning principle of the UWB sensors is deepened, drawing particular attention to ranging techniques, main sources of error and trilateration algorithms.

In the second part of the work, some experiments are carried out to evaluate the performance of the proposed system. Several measurements are performed using a commercial set of UWB sensors from Decawave. The localization accuracy is evaluated through ranging and positioning measurements. The computed parameters are then used in simulation in combination with information on the positioning of a drone hovering in fixed position. In this way it is finally possible to compute the expected error in the localization of the ground vehicle.

Table of contents

List of figures

List of tables

Chapter 1

Introduction

The aim of this thesis is to develop a UWB based multi-robot cooperative localization system capable of efficiently navigating a UGV in partially GPS-denied environments, which is a crucial issue for several applications such as agriculture and search and rescue. Typical robotic outdoor navigation critically relies on the localization service provided by the Global Positioning System, which suffers from the multipath effect and blockage of line-of-sight. [8] Thus, alternative techniques must be taken into account if unmanned vehicles need to operate when they are hidden from satellites, for example by canopies in woods or orchards, or when obstacles such as tall buildings interfere with GPS signal.

Common approaches for the estimation of the position of mobile robots are based on visual odometry (VO) [3], simultaneous localization and mapping (SLAM) and preinstalled beacon-based localization. Kia et al. [12], Kim et al. [13] The first two methods are affected by significant position drift error for long-time navigation [1], instead having fixed nodes working as anchors means that some kind of infrastructure is needed, moreover the working area is geometrically limited. Kim et al. [13] proposed a solution involving two drones equipped with cameras aiding an UGV to steer around. In these systems the drones are capable of detecting obstacles, but they are not useful in precisely localizing the rover.

To deal with the localization problem, a system that merges together the potentiality of cooperative robotics and UWB technology is proposed. In our set up three drones or more are hovering above the working area and act as mobile anchor nodes, while the rover is located measuring the relative position of all agents. The UAVs can fly above obstacles, their position is therefore measured using GPS. UAVs and UGV are continuously exchanging data package through UWB, so their relative position is known in real time. With this information a trilateration algorithm can be used to compute the location of the rover, moreover knowing the relative distance between the drones, it is possible to improve the precision of their absolute position. [12]

As the first stage of development of the system, this experimental work aims at evaluating which is the best possible accuracy we can obtain in the localization of the UGV. The distances between the anchors and the tag node are measured by means of the commercial ultra-wide band evaluation kit Decawave TREK1000. The sensors are characterized taking several ranging and positioning measurements both in line of sight and non-line of sight. Moreover, an error analysis of the positioning of a drone hovering in fixed position is performed using data coming from other experiments. Thanks to all this information, the whole system is simulated in order to estimate the expected error and to evaluate the best position for the anchors.

Chapter 2

Localization techniques

"Locating is a process used to determine the location of one position relative to other defined positions and it has been a fundamental need of human beings ever since they came into existence." [4] Since the dawn of humankind the desire to explore and control the environment motivated the development of several techniques and tools based on observation of the stars in order to allow open sea navigation and to set land boundaries. One of the first instrument that made it possible to measure the location of a point on the earth was the astrolabe. It was developed by the Greeks in the Hellenistic era and then perfected by the Arab. Since then a lot of sophisticated techniques were developed to permit the sailors to explore the globe, but they still relied on the on the same astronomical principles. The real revolution in the field of navigation and localization became true only in the technological era with the advent of radio transmissions. The most popular positioning system that exploits wireless transmissions is the Global Positioning System (GPS). It is based on satellites and has been fully operational since 1994, allowing whoever possess a ground receiver to discover its location with meter accuracy. Other radio technologies that can be used to compute the position of a device include the Global System for Mobile communications (GSM), Wireless Local Area Network (WLAN), Wi-Fi and Wireless Sensor Networks (WSN). The possibility of knowing the exact position of a person, an autonomous vehicle, a device, etc. allows the introduction of several services such as personnel tracking, navigation assistance, security alerts, informational and entertainment applications. This kind of services are called Location Based Services (LBS) and they are becoming more and more common in our everyday life. Some applications nevertheless require a much higher positioning accuracy then others to be effective, motivating the adoption more than one of the previous technologies at the same time or even the development of ad hoc localization systems. This is the case of mobile robotics in which navigation is one of the most important tasks to accomplish. Navigation can be defined as the combination of three basic operations: self-localization, path planning

and map building. [14] This is much more complex than just knowing the position of the robot, but is self-evident that precise positioning is essential to set up a robust navigation system. In this thesis we propose a hybrid localization system exploiting GPS and Ultra-Wideband (UWB) sensors in order to aid the navigation of an unmanned vehicle in partially GPS-denied environment. In the first part of the present chapter, a classification (as proposed by Zekavat and Buehrer [25] and Dardari et al. [4]) and a brief description of the most common localization technologies is proposed. The last subsections, instead, are dedicated to the detailed description of the novel technique that we are studying.

2.1 Classification of Wireless positioning systems

2.1.1 Classification based on reference frame

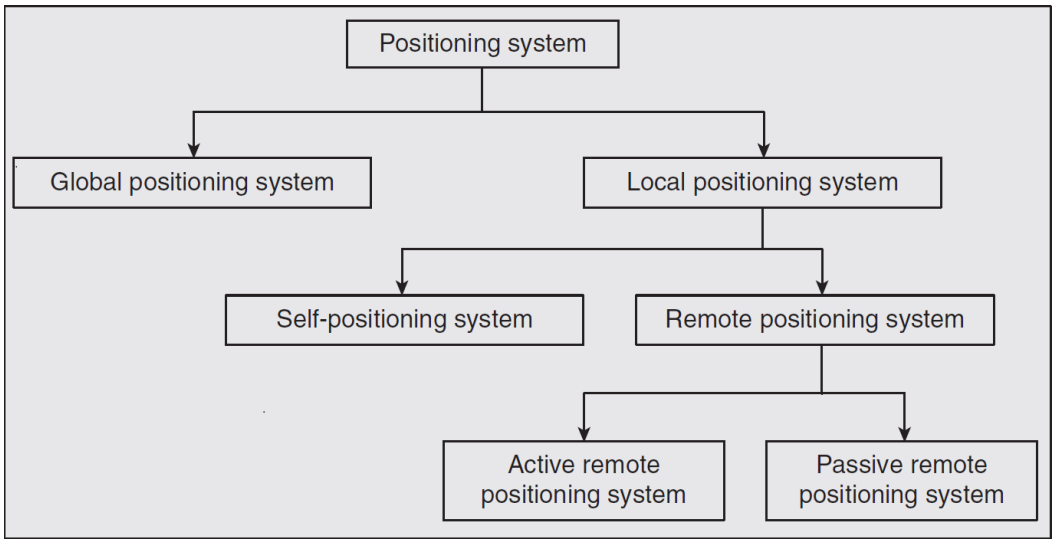

Fig. 2.1 General classification of positioning systems. Source: Zekavat and Buehrer [25]

In Figure 2.1 a very general classification of the positioning systems based on the reference frame is shown. It is possible to distinguish two main categories:

- *Global positioning*: permitting the user to find his position on the globe, usually in terms of latitude and longitude (absolute reference frame).
- *Local positioning*: allowing the target to know the position relative to some infrastructure or landmark (relative reference frame).

Local positioning systems can be further divided in self-positioning and remote positioning. The first gives the target the chance of finding its position with respect to a fixed point in

any time and location (e.g. Inertial Navigation System). The second allows to reconstruct the position of a node relative to the position of other nodes in the coverage area. Within remote positioning systems it is possible to point out other two subgroups:

- *Active target remote positioning*: in which the target actively participates in the process of the localization exchanging information with other nodes, for example radio frequency identification (RFID) and wireless local positioning systems (WLPS).
- *Passive target remote sensing*: the target doesn't cooperate in the positioning procedure. Typical examples are tracking radars and vision systems.

From now on the term "wireless positioning systems" will indicate only the active ones. The passive systems makes use of very different functioning principles than the active ones and the applications are quite different too, although this topic is not dealt with in the present study.

2.1.2 Classification based on type of measurements

Table 2.1 Classification based on type of measurements

Measured Quantity	**Positioning Scheme**	**Characteristic Aspect**
Angle of arrival (AOA)	Angle based	Characterizes the direction of propagation Usually antenna arrays are required
Received signal strength (RSS)	Range based Fingerprinting Interferometric	Measurement of the received power
Time of arrival (TOA)	Range difference based	Measurement of the signal propagation delay
Near-field ranging (NFR)	Range based	Relates the distance to the angle between the electric and magnetic fields in near-field conditions
Radio visibility	Proximity range-free	Connectivity

The positioning process typically consist of two phases: firstly some kind of measurement are performed between nodes, secondly this information is used to compute the position

using different types of algorithms. A more detailed classification based on the type of measurements that are carried out to perform the localization is shown below and is summed up in Table 2.1.

The most common ranging techniques are:

- *Angle-of-Arrival (AOA)*: this technique is based on the measurements of the angle of the arriving signal. The source of the signal lies on the straight-line passing through the measurement station and with the measured angle. Hence, in a coplanar case, only two anchor nodes (three in a 3D scenario) are needed to obtain the position of the target as the intersection of the two lines. In order to measure the AOA, the anchor nodes should be equipped with antenna arrays that are typically complex, expensive and power consuming.

- *Received Signal Strength (RSS)*: the possibility of measuring the received signal strength is available in almost every wireless device. Exploiting the basic concept that the signal tends to progressively fade away when the distance from the source increases, it is possible to perform an estimation of the distance between an anchor node and the target. Once the distance from three or more anchor nodes is available the position is obtained using trilateration. There are several theoretical and empirical models that provide a ranging estimation given the difference in dB between the signal power at the source and at the receiver, but they are all affected by signal propagation issues such as shadowing, refraction, reflection and multipath effects. Another positioning method based on RSS is called fingerprinting. In this case a map of the signal power is built during the calibration phase. The position of the target node is then obtained matching the measured value and the data contained in the map.

- *Time-of-Arrival (TOA)*: as known, electromagnetic waves travel at the speed of light ($c = 3 \cdot 10^8 m/s$). So, by measuring the time of flight (TOF) τ of a signal from the transmitter to the receiver, it is possible to compute the distance between the two devices as $d = \tau \cdot c$. If at least three anchor nodes (four in 3D positioning) are available, it is possible to compute the position of the target as the intersection of the three circles centered in the anchors position and having the radius equal to the measured distance. The main problem with this technique is that very precise time measurements are needed and the clocks of all the devices must be synchronized. A method to overcome this issue is called Time-Difference-of-Arrival. It consists in measuring the delay with which the signal transmitted by the target reaches two anchor nodes. In this way the clock of the transmitter does not need to be synchronized with the others. The position

required lies on the hyperboloid having the anchor nodes as foci, so, using three base nodes, the point can be determined as the intersection of the two curves.

- *Connectivity*: this is the simplest way to obtain information on the position of a wireless device. The only information used to perform localization is whether the connection with the anchor nodes is available or not, thus there is no need to use dedicated hardware and time synchronization. On the other hand, using only proximity information lead to a poor positioning accuracy.

- *Near-Field ranging (NFR)*: in this case, the measured physical property used to estimate the distance is the difference between the phase of the electric (E) and the magnetic (H) fields of the received signal. Indeed, in the proximity of small antennas the phase shift between E and H is 90°; as the distance from the source increase the phase difference becomes smaller tending to zero in the far-field. This technology exploits low frequency signals (530-1710kHz) that guarantee high penetration capabilities and a better immunity to multipath effects. Moreover, this methods does not need the synchronization between the transmitter and the receiver, but is suitable only for distances below 30-65 m. [22]

2.1.3 Classification based on network configuration

Table 2.2 Classification based on network configuration

Network Configuration	**Characteristic Aspect**
Anchor-based	Some nodes know their locations
Multihop	The distance from anchors can be obtained indirectly by means of intermediate nodes
Single-hop	The distance from anchors can be obtained by direct interaction
Anchor-free	None of the nodes knows its position. Only relative coordinates can be found
Range-free	Only connectivity information is used
Terminal-centered	Specialized electronics within the mobile handset to determine its own location
Network-centered	Specialized location equipment within the network to determine mobile terminal's location

The nodes constituting the wireless positioning systems are of two types: the ones that are aware of their position being placed at known locations or equipped with GPS (anchor nodes or beacons) and the ones that need to estimate their position communicating with the anchors (agent, target nodes or tags). Depending on the number and the deployment of the nodes, it is possible to distinguish different types of networks. If the agent can communicate with a sufficient number of anchors, then it is possible to adopt *single-hop* algorithms. On the other hand, if this is not the case, the agents must cooperate to in a *multi-hop* fashion to propagate the information and allow the localization. In other situations if none of the nodes are at a known position, thus it is possible to compute only the relative location of the elements of the network. This is called *anchor-free localization*. Finally, there is the distinction between *terminal-centered* and *network-centered* systems. The firsts are characterized by the capability of the target nodes to compute their position autonomously once they have acquired the distance measurements. In the other case the signal transmitted by the agent is used by the anchor nodes to compute the location and the information is then sent back to the agent.

2.2 Global navigation satellite systems

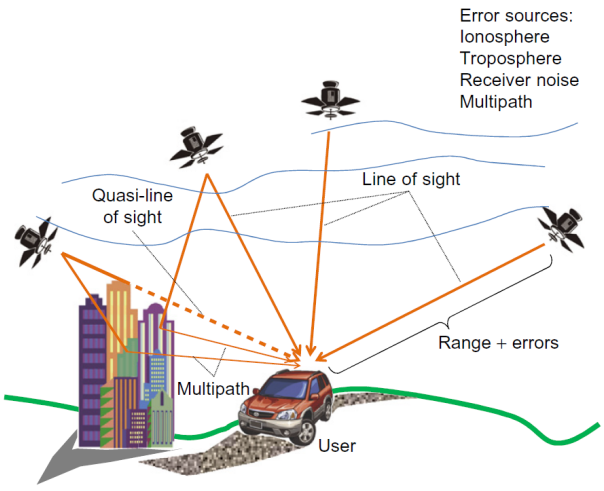

Fig. 2.2 Basic GPS functioning. Source: Dardari et al. [4]

The main aim of a GNSS is to allow the user to estimate his own position on the globe usually in terms of latitude, longitude and height. The localization process is based on range measurement, in theory only three satellites are needed. The position of the receiver is obtained as the intersection of three spheres centered on satellite and having the radius

equal to the range measurements. However, modern receivers are equipped with inexpensive crystal clocks which are set approximately to system time. Thus, there is an offset between the ground receiver and the true system time and this leads to a difference in the measured distances and the geometric range. The measured quantities are called pseudoranges R and they include the real distance ρ plus a range correction $\Delta\rho$ due to the clock bias δ.

$$R = \rho + \Delta\rho = \rho + c\delta \tag{2.1}$$

Where c is the speed of light. [10]

Using pseudoranges, four measurements and so four satellites are needed. In fact, in this case, the unknown are the three coordinates and the clock bias.

With regards to the basic components of a GNSS it is possible to identify three main segments: the *space segment* that is a constellation of satellites transmitting on-way radio signals which contain the current satellite position and time; the *control segment* that has the purpose of maintaining the health status of the constellation keeping the satellites in the wright orbit and adjusting their internal clocks; the *user segment* which consist in the GPS receiver device that is able to compute the user location trough the information coming from satellites. [4]

2.2.1 Existing satellite-based positioning systems

Nowadays GNSSs are essential for a large number of applications from defence an civil protection to leisure and commercial activities justifying the development of several satellite constellations promoted by different countries. Hereafter, a list of the main GNSSs with the main characteristics of each system is reported.

- *Global positioning system*: the GPS constellation consist of 31 satellites positioned on six earth-centered orbital planes with five to six satellites on each plane. The nominal orbital period of a GPS is one-half of a sidereal day (approximately 11 h 58 min). The orbits are nearly circular and equally spaced about the equator at a 60° separation with a nominal inclination of 55° relative to the equator, whereas the orbital radius is approximately 26,600 km (20,200 km average height above ground). The GPS constellation provides a 24-h global user navigation and time determination capability. From its very inception, the GPS was meant to provide two services, corresponding to two different signal formats: the standard positioning service (SPS) and the precise positioning service (PPS). The SPS is designed for the civil community, whereas the PPS is slated for the United States authorized military and selected government

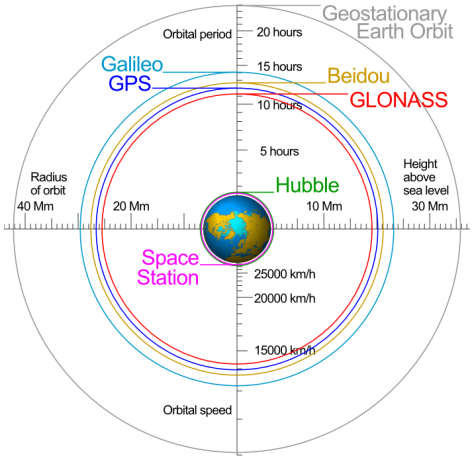

Fig. 2.3 GNSSs orbits. Source: *spotlight.unavco.org*

agency users. The nominal accuracy of the SPS, considering a global average, is 13m, 95%, for horizontal positioning and 22m, 95%, for vertical positioning. However, real performance is often much better reaching values of 3.0 m and 4.3 m respectively. [4, 9]

- *Galileo*: this is a project promoted by the ESA (European Space Agency) and the EC (European Commission) in order to develop a self-standing satellite based positioning system. Both Galileo's space segment and ground segment are independent from other systems, but they are designed to be compatible and interoperable with other radio navigation satellite systems like GPS and GLONASS. The project stared on May 26, 2003 and the first two GIOVE (Galileo In-Orbit Validation Element) satellites were launched by ESA in 2005 and 2008. They served as testbed for key technologies such as onboard atomic clocks and navigation signal generation. These two satellites have been dismissed and moved to higher altitudes. The development of the space segment is still an ongoing process; the first GALILEO services have been available since 2016, but only in 2020 will it become fully operational with a constellation of 30 satellites (24 operational plus 6 spare). They will be placed on three equally space medium earth orbit (MEO) planes with an inclination of 56° with reference to the equatorial plane and an average orbit semi-major axis of 29,600.318 km. The constellation geometry has been designed to achieve optimal geometric conditions all around the globe, providing better coverage in higher latitudes when compared to GPS. [9] Galileo is thought to provide five different services: an open service (OS) providing all information such as positioning, navigation, and timing services; a safety of life (SoL) service compliant with the needs of safety critical users such as civil aviation, maritime, and rail domain; a commercial service (CS), aimed at generating commercial

revenues through the provision of added value over the OS; a public regulated service (PRS), for application devoted to European and member states, in particular for critical applications and activities of strategic importance (defense/civil protection); a search and rescue (SAR) service providing assistance to the COSPAS-SARSAT system by detecting emergency beacons and forwarding return link messages to the emergency beacons. [4]

- *GLONASS*: like GPS and Galileo, GLONASS is based on several ground stations that monitor and control the satellites and their signals. The GPS and Galileo stations are spread on the globe, to guarantee a better control of the constellation and its signals. On the contrary, for political and military reasons, the GLONASS ground segment is completely located inside the former Soviet Union territory, since the Soviet Union never had territories or trusted allies abroad. This geographic concentration is a weakness of GLONASS because it reduces the precision and the efficiency of the whole system. The full GLONASS space segment consists of 21 operational satellites plus 3 spare satellites located on three different orbital planes spaced by 120°. The satellites within the same orbit plane are separated from one another by 45°. The orbits are circular with an inclination angle of 64.8°, and the orbital height above ground level is about 19,140 km (i.e., slightly lower than the GPS satellites). The orbit period is 11 h and 16 min. The whole constellation has a revolution period of 8 days. The 24-spacecraft constellation is currently undergoing modernization, with the progressive replacement of old-generation satellites with new-generation ones. The GLONASS constellation will ultimately be expanded to 30 satellites, although this will require an upgrade to the control segment, which currently can handle only 24 spacecrafts. [4]

- *BeiDou 2*: Compass is the incoming Chinese GNSS. China started the development of an autonomous GNSS in the 1960s, but only during the 1980s did the project actually gain momentum. In 1994, China approved a new satellite system for navigation purposes on the basis of the radio determination satellite service (RDSS), a technology from GPS. The first Chinese system was named BeiDou, from the Chinese name of the Northern Star, the brightest star of the Ursa Minor constellation. BeiDou was born like a regional dual system (both military and civil), to provide navigation and timing to China and surrounding areas. The evolution of the BeiDou system is called BeiDou-2 or, more commonly, Compass. The first satellite of the Compass navigation satellite system (CNSS), which is a MEO satellite, was launched in April 2007. It started covering China and parts of neighbouring countries in 2008 and will develop into a global constellation step by step.

2.3 Local positioning systems

The increasing interest in local positioning systems (LPS) is motivated by the large development of LBSs which require that the positioning devices can work seamlessly in a variety of critical conditions like inside warehouses, multi-storey buildings, underground stores and parking areas, agricultural environments and woods. In all these situation GNSSs fail or give very poor performances in terms positioning accuracy. In fact, the presence of obstacles such as walls tall building and trees, produces some harmful effects such as blockage of line of sight between the satellites and the receiver, signal power attenuation and multipath propagation. Thus, to satisfy the needs of the final user, LPS are used as complementary or standalone solutions when GNSS alone is no sufficient.

As shown in paragraph 2.1, LPSs can differ a lot from each other in terms of network architecture, positioning techniques and devices used, but they are all made up of some base node at known positions and one or more target node to be located. Most LPS are a sort of by-product of existing wireless telecommunication networks like GSM, WLAN and Wi-Fi, so in this case localization is an auxiliary service with respect to data communication. However, in recent times, several dedicated Real Time Localization Systems (RTLS) based on RFID and UWB have been developed too.The main difference between LPS and GNSS is that their coverage area is limited to the region in which the base nodes, that are typically fixed on the ground, are deployed.

The following list reports the main LPSs and their main characteristics.

- *Cellular networks*: these systems rely on a set of base stations (BSs), with a coverage radius of up to about tens of kilometers each. Nowadays they are widely deployed in all developed countries. The most widespread positioning technology in cellular networks is based on TDOA. For instance, GSM location is based on the existing observed time difference (OTD). OTD evaluates the time difference between signals traveling from two different BSs to a mobile device. At least three visible BSs are needed to estimate the position of the target node, obtained by intersecting hyperbolic lines having foci at the BSs' positions. The final location estimation accuracy in GSM-based location systems using OTD ranges from 50 to 500 m. The signal parameter estimation method used in UMTS networks is the observed TDOA (OTDOA), which is based on the TDOA approach. Anyway, the accuracy of cellular-based positioning is quite modest, for this reason recent location estimation algorithms try to exploit any available information about the environment (e.g., fading conditions, Doppler frequency, and network topology) to attain higher accuracy through data fusion methods.

- *Wireless LANs*: WLAN indoor locations are deployed in much smaller areas than in cellular networks. They are widely used both in private and public facilities such as company campuses, universities, corporations, airports, museums, and shopping malls. Outdoor WLANs' deployment can be seen only in small zones of large cities as hot spots. WLAN-based positioning solutions rely mostly on signal strength evaluation. Since received signal strength (RSS) measurement is part of the normal operating mode of a wireless transceiver, no other ad hoc hardware infrastructure is required. The most used WLAN positioning techniques exploit fingerprinting methods.

- *Radio Frequency Identification*: this technology has attracted an enormous interest worldwide, since the earliest pioneering ideas dating back to 1948. A number of applications can now be found in several fields such as logistics, automotive, surveillance, automation systems, and in general real-time object identification. An RFID system consists of tags applied to objects and their readers. The reader interrogates the tags via a wireless link to obtain the data stored on them. When tag cost, size, and power consumption requirements become particularly stringent, passive or semipassive tag solutions are taken into consideration. Communication with passive tags usually relies on backscatter modulation, and the tag's control logic and memory circuits obtain the necessary power to operate from the RF signal sent by the reader. Recent developments indicate a trend to hybridize active RFID and RTLS technologies. Some RFID vendors are adopting or adapting RTLS concepts to provide additional functionalities for their products. Several systems rely on proximity-based positioning algorithms, which, in general, are not very accurate for many applications. Some research efforts are also going on to merge RFID and UWB technologies toward extremely low-cost RTLS. Positioning algorithms adopted in RFID-based RTLS are usually the same as those adopted in WLANs and WSNs.

- *Wireless sensor networks*: A WSN in its simplest form can be defined as a network of (low-size and low-complex) devices denoted as nodes that can sense the environment and communicate the information gathered from the monitored field through wireless links. The data are forwarded, possibly via multiple hops relaying to a local sink (a controller or monitor) or to other networks through a gateway. The number of applications where WSNs are used today, or has been envisioned for the future, is quite large. Apart from the "core" applications regarding general monitoring of environment or processes, WSNs are or will be used also for applications in traffic safety, medicine, agriculture, logistics, and disaster relief, to name but a few. In many (not to say all) WSN applications, a sensor reading is not of much use unless

it is accompanied by the position at which the data were gathered. The positioning problem in WSNs can vary widely in character from network to network, and from application to application. The appropriateness of the approach to positioning for sensor nodes depends on the available hardware, measured data, infrastructure, and on the application requirements. In some cases, a fixed infrastructure can be installed throughout the network deployment area in order to aid the positioning of mobile sensor nodes. This infrastructure may include reference nodes at known location (anchors), or central processing stations with extended resources in terms of computational power and/or energy supply. The expected size of the network, that is, the node density and the coverage area of the network, also plays an important role in the design process. Some WSNs that have been envisioned in the literature involve thousands of sensor nodes densely spread out over very large areas. In such large networks, it is of paramount importance that the complexity of the positioning algorithm is not a rapidly increasing function of the number of nodes and/or connectivity level of the network; that is, algorithm scalability is often an important factor to consider.

- *Ultra-wideband*:UWB is promising for high-definition indoor positioning, as it can achieve very accurate short distance estimation. UWB is also a viable technology for short-range wireless indoor communication with a number of attractive potential features: high-rate transmission, low complexity, low cost, and low power consumption. The traditional design approach for a UWB communication system uses baseband narrow timedomain pulses of very short duration, typically of the order of a nanosecond, thereby spreading the energy of the radio signal quite uniformly over a wide frequency band ranging from extremely low frequencies to a few gigahertz. This method is usually called impulse radio UWB (IR-UWB). A great advantage of the short pulse modulation is the possibility to estimate the TOA with a fine resolution, which translates in ranging estimation with an accuracy of less than one meter. The functioning of UWB devices is deepened in Chapter 3.

2.4 Navigation in GPS-challenging environments

When dealing with mobile robotics, the main objective is to develop robots that are capable of moving autonomously in unknown environments. The basic approach to the outdoor navigation is to exploit the global navigation satellite system (GNSS). Nevertheless, there are a variety of scenarios in which this solution doesn't provide a sufficiently precise estimation of the robot position. For example, when the navigation is performed in an urban canyon, the presence of tall buildings can cause complete GNSS blockages or at least severe multipath

effects leading to positioning errors as large as hundreds of meters. [21] The same type of limitation can be found in other applications such as agriculture and search and rescue, as a matter of fact, the presence of dense canopies in orchards and woods is sufficient to make the global positioning system ineffective. These scenarios are a few of the better-known cases in which alternative technologies to GPS must be taken in to account. Other potential applications include the use of autonomous robotic systems for bridge inspection or structural health monitoring, surveillance applications in urban environments, or applications that require robots to transition from indoor-to-outdoor operations or vice versa. [21]

2.4.1 State of the art

To overcome the difficulties related with GPS-challenging situations several solutions have been studied. Two of the most common techniques make use of inertial measurement units (IMU) and cameras. The first is called visual odometry (VO), which is a procedure of incrementally estimate the position and orientation of the navigating vehicle by analyzing the deviation that the motion induce on the sequence of images captured by the one or more on-board cameras. [3] The second method is simultaneous localization and mapping (SLAM): this type of algorithm incrementally builds a consistent live map of the surrounding environment and estimates the pose of the vehicle by matching between the real-time map of the vehicle with the surrounding environment recently captured. [3] Using cameras to preform navigation has some advantages: the sensors are light-weight and low-power and can be used at the same time to perform other tasks such as surveillance. On the other hand, both VO and SLAM are affected by significant position drift error for long-time navigation. [1]

Another solution is based on preinstalled RF beacon. In this case there are two methods to estimate the position of the robot: range-based and range-free localization. The first relies on distance or angle measurements and the position is computed using trilateration, triangulation or other specific algorithms. The second method uses the information of topology and connectivity for location estimation. [20] Typically, these techniques are used in indoor environments when a very precise estimation of the position is needed, but it is also used outdoor both with pre-existing wireless sensor networks (WSN) or with ad hoc networks. [8, 20, 23] The convenience of this kind of system reside on the possibility of exploiting already available facilities and the good accuracy that could be achieved. The main drawback is the necessity of some kind of infrastructure that is often unavailable outside of urban environments and is a geometrical boundary for the motion of the autonomous vehicle itself.

Finally, one of the most promising technologies is cooperative navigation. [21] Cooperative means that there is a group of mobile robots (that can be both flying or ground vehicles)

which can exchange information about their relative distances and these measurements are used as a feedback signal to increase the accuracy of the position estimation of each member of the team. [12] This technique is particularly suitable when dealing with partially GNSS-denied environment, that is when the signal is not completely blocked but is too weak or temporary unavailable for one or more agent. The particular appeal of cooperative localization relies on the fact that sporadic access to accurate localization information by a particular robot results in a net benefit for the rest of the team. [12] Moreover, the system is particularly flexible because it does not need any auxiliary infrastructure. The main disadvantage is that, contrary to VO and SLAM, the access to the GPS is still required, so the system by itself will not work indoor.

2.5 Multi-agent localization system description

2.5.1 Working scenario

Obviously, each of the solutions described in the previous paragraph has its pros and cons and the choice of one system or another should be made taking into account the scenario in which the autonomous system will work and the tasks it will have to accomplish. The object of this thesis is to examine an innovative cooperative localization system that has been thought to deal with the navigation in agricultural environments. In particular, our goal is to localize an autonomous ground vehicle that can perform different kind of activities (e.g. spraying, plant monitoring,...) in vineyards and orchards. Knowing the precise position of the UGV is a crucial issue in this kind of application both for the safety of the machinery itself and to avoid damage to the plantations. As mentioned at the beginning of this chapter, this is a typical situation in which the GPS can fail. Moreover, pre-existing infrastructure that could aid the navigation are typically completely absent in rural contexts and the installation of a dedicated WSN in such large areas is expensive and it requires periodic maintenance. With this in mind, the adoption of a cooperative navigation system seems to be the best approach. Furthermore, the flexibility of this kind of system makes it suitable to guarantee the localization of any type vehicle or device even in environments that are different from the agricultural one.

2.5.2 System setup

The team of robot that constitute the proposed cooperative localization system is made up of three or four quadcopters and one ground vehicle. While the UGV is performing its tasks in the orchard, the drones fly over the work area so they can be localized using GPS. Moreover,

Fig. 2.4 Multi-robot localization system setup

all the robots are equipped with ultra-wide band sensors that permit to measure the relative distance between them with centimetre-level accuracy. By using all this information it is possible to compute the location of the rover by means of trilateration or multilateration algorithms (see Chapter 4). In principle the team of robots can be extended if a larger plot of land has to be covered or additional ground vehicles work at the same time. Moreover, the possibility of dynamically placing some UWB beacons within the work area will be studied in the future. The idea is to provide the UGV with a certain number of sensors that can be dropped on the ground once the position of the rover itself has been computed. In this way it is possible to build a local network of anchors that still aids the navigation when the support of the quadcopters is no longer available.

The performance of the whole system strictly depends on an accurate knowledge of the position of the UAV, so it is advisable to adopt dual frequency GPS or RTK-GPS, even if they are more expensive than the standard sensors. Moreover, other kind of aerial vehicle could be considered, but, at this very early stage of the development of the system, the ability of quadrotors to fly in a fixed position and their dexterity seems to guarantee several advantages. The choice of the type of UAV conditions the strategy that is adopted to position the anchors in order to optimize the accuracy of the localization. Some considerations on this topic are made further on in this document, however the study of a specific algorithm for the dynamic positioning of the drones will be examined in the future.

Chapter 3

Ultra-wideband for localization

3.1 Brief History of UWB

Contrary to what might be thought, the very first wireless communication systems were based on ultra-wideband signals. UWB, indeed, is often perceived as a recent technology compared to narrow-band radio transmissions, quite the opposite its first application is dated back in 19th century. In fact, in the spark gap transmitter (Figure 3.1), designed by Marconi in the 1890s and based on the previous works of Hertz, the radio waves were generated by means of an electric spark; hence, the signal was composed of short pulses with a very high bandwidth. After the first real world application of the spark gap transmission in June 1896, the system started to become quite common and the first problems arose: due to the large radio spectrum occupied and the lack of syntony circuits, two station could not operate in the same geographical region. The development of the UWB was quickly abandoned in 1910s with the advent of vacuum tubes communication. Since then wireless communications have been dominated by continuous wave radio transmissions. A new interest in UWB technology started in the late 1960s motivated by the need of developing low probability of detection wireless transmissions for military purposes. [17] The application of this technology was restricted to military and Department of Defence applications under classified programs 1994 when some of the patents were unclassified.[18] As interest in the commercialization of UWB has increased over the past several years, developers of UWB systems began pressuring the U.S. Federal Communications Commission (FCC) to approve UWB for commercial use. In February 2002, the FCC approved the First Report and Order (R&O) for commercial use of UWB technology under strict power emission limits for various devices, in order to avoid harmful interference with existing systems. In 2006, European Commission permitted the unlicensed use of UWB technology in shared frequency bands too, even if with slightly more stringent regulation.[15, 25]

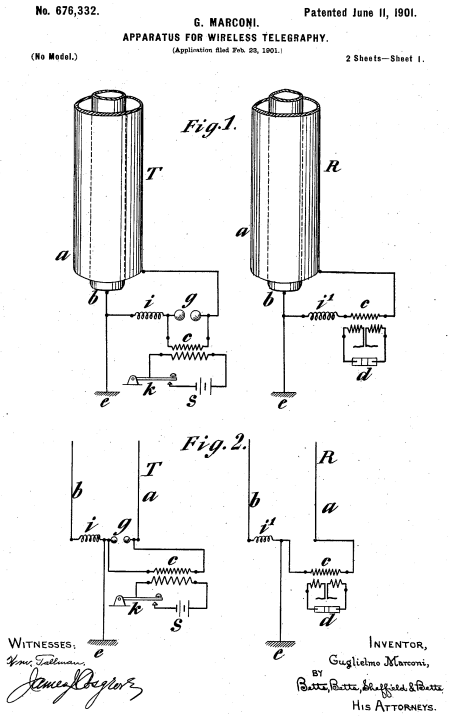

Fig. 3.1 Illustration of the spark-gap transmitter from the original patent of G. Marconi

3.2 Definition and regulation

As mentioned in the previous section, in 2002 the U.S. FCC permitted the unlicensed use of UWB technology in the frequency range of 3.1-10.6 GHz. The FCC definition of UWB signals states that they should occupy a 10 dB bandwidth grater of 500 MHz or have a fractional bandwidth exceeding 20%.

$$FractionalBandwidth = \frac{2(f_H - f_L)}{(f_H + f_L)} \geq 20\% \tag{3.1}$$

where f_H and f_L are respectively the upper and lower frequency limits of the 10 dB bandwidth. [16]

UWB must coexist with other communication systems, technologies and services operating in the same allocated bands, so it is required that the power emission levels of the UWB signals must be sufficiently low to avoid interference. The FCC imposes specific operational limitations depending on the different applications, including imaging systems, vehicular radar, indoor and handheld UWB systems. For example, the power spectral density emission limits for indoor application are set to -41.3dBm/Mhz in the band between 3.1 and 10.6 GHz as shown in Figure 3.2a. Europe has adopted a different UWB regulation approved

by the EC's Radium Spectrum Committee that identifies the frequency bands of 3.4-5.0 GHz and 6.0-8.5 GHz, potentially extendable up to 9 GHz (Figure 3.2b). In addition, the last regulations impose supplementary restrictions to the utilization of UWB devices. For example, in outdoor environments, UWB systems should not include fixed transmitter and they can't be use in vehicles. [17]

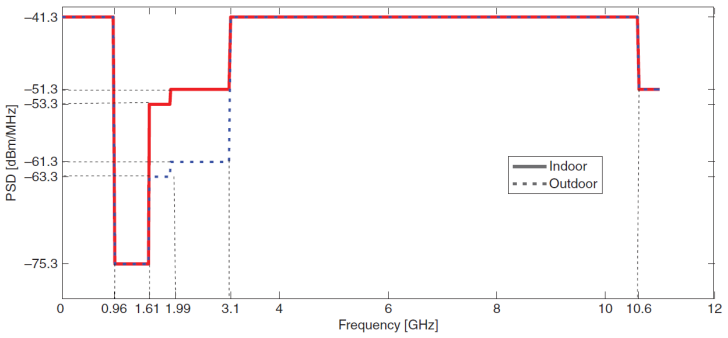

(a) UWB spectral mask as defined by FCC

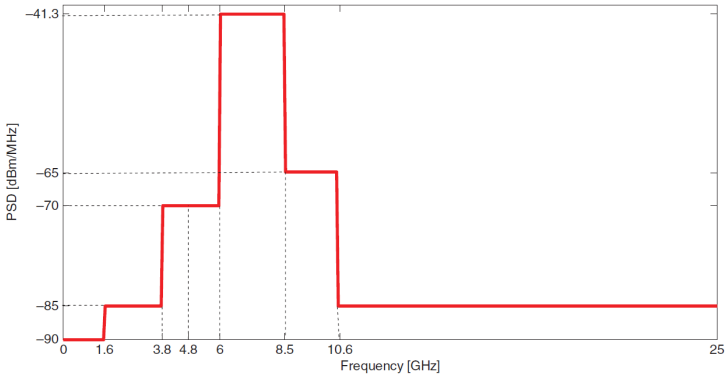

(b) European UWB spectral mask

Fig. 3.2 UWB emission limits

3.3 Advantages

Compared to continuous wave (CW) systems, UWB present many advantages directly related to the physical properties of the transmitted impulse signal. UWB makes use of short-duration (nanoseconds to picoseconds) pulses that present a much wider instantaneous bandwidth than that of CW systems. These signals contain both high and low frequency components and this makes them particularly suitable when fine-range resolution and long range are required. Indeed, the range resolution is inversely proportional to the bandwidth and the low frequency

components guarantee a long propagating distance as well as high penetration capabilities through a large variety of materials, including walls. [15] The very high bandwidth guarantees also a reduced signal diminishing in environments with severe multi-path fading or when there is an excessively high signal attenuation at some frequencies. Moreover, the mean average transmitted power of UWB impulse system is typically very low, producing low interference to the existing or co-operating RF systems. Another important property is the high multi-path resolution. As a matter of fact, when a signal with a very narrow pulse width is reflected, it has a very short time-window of opportunity to collide with the line-of-sight signal and cause signal degradation. Last but not least, the narrow time duration of pulse signals leads to a very high timing accuracy, when, for example, measuring the ToF of the signal. This makes UWB systems particularly suitable for precise locating systems. [16]

3.4 Theory of UWB

Every UWB system is constituted of at least three basic components:

1. *The transmitter*: that produces the radio signal emitting electromagnetic waves.
2. *The wireless channel*: that is the medium through which the signal propagates.
3. *The receiver*: the device that receives and interprets the transmitted signal.

The signal that reaches the antenna of the receiver will be in some way modified with respect to the original transmitted wave. This depends on the characteristics of the channel that is the environmental conditions. In order to describe the received signal, what is needed is the input signal produced by the transmitter and the channel impulse response (CIR). From a mathematical point of view, the received signal $y(t)$ is given by the convolution product of the CIR $h(t)$ and the input signal $x(t)$:

$$y(t) = h(t) * x(t) := \int_{-\infty}^{+\infty} h(\tau)x(t-\tau)\mathrm{d}\tau \tag{3.2}$$

A more detailed explanation of the functions describing the CIR and transmitted signal is given respectively in Section 3.4.1 and 3.4.2.

3.4.1 Channel model

Generally speaking, there are two main approach to model a wireless channel: deterministic models and stochastic models. In the first case, if the geometries and the electromagnetic

properties of the materials in the surrounding area of the transmitter are known, it is possible to exactly solve the Maxwell's equations. In this way one can obtain a prediction of the CIR relative to the operating environment. Stochastic models, on the other hand, try to model the "typical" properties of a wireless channel, without taking into account the specific location. [6]

The most common approach to model the ultra-wideband propagation channel is the stochastic one. [25] A very simple model is given by the following equation [17]:

$$h(t) = \sum_{n=1}^{N} a_n \delta(t - \tau_n) e^{j\theta_n} \tag{3.3}$$

where N is the number of multi-path components and a_n, τ_n, and θ_n are respectively amplitude, delay, and phase of the nth component. If the UWB signal is a base band signal the phase parameter in Equation 3.3 can be omitted. [17]

It is evident that $h(t)$ is basically a summation of a finite number of Dirac delta functions, where the parameters are statistically determined by real world measurements. Some observations about the effects of the CIR on the input signal can be easily made looking at Equation 3.3 in combination with the properties of the Dirac delta function δ. The shifting property states that

$$\int_{-\infty}^{+\infty} x(t)\delta(t - t_0) = x(t_0) \tag{3.4}$$

so, preforming the convolution product between $\delta(t - t_0)$ and the signal $x(t)$ the result is

$$x(t) * \delta(t - t_0) = x(t - t_0) \tag{3.5}$$

which means that the convolution of a signal with a Dirac pulse located at t_0 is the same signal shifted in time of t_0. Taking in to account a base band signal, thus ignoring the parameter θ in the Equation 3.3, it is clear that the received signal, given by the convolution between $h(t)$ and $x(t)$, is the summation of N time shifted version of the input signal weighted by the relative parameter a_n. Intuitively, this is exactly what happen in a multi-path environment where the signal is reflected by walls or other obstacles and hits the receiver antenna with different time delay. One of the biggest advantages of UWB is that, thanks to the use of extremely short pulses, the direct path signal is easy to detect having a minimal overlap with the other components. [5]

For sake of completeness, the model proposed by Saleh and Valenzuela (S-V) in 1987 is reported. This model or slightly modified versions are the most used to describe the

UWB channel. In this case, the fact that multi-path components come in clusters is taken into account and so the channel is modelled with a double Poisson process. [5, 25] The mathematical formulation of the CIR is the following [25]:

$$h(t) = \sum_{m=0}^{+\infty} \sum_{n=0}^{+\infty} a_{m,n} e^{j\theta_{m,n}} \delta(t - T_m - \tau_{m,n}) \tag{3.6}$$

where $a_{m,n}$ and $\theta_{m,n}$ are the multi-pah amplitude and phase as before. T_m is the arrival time of the first path of the mth cluster and $\tau_{m,n}$ is the delay of the nth ray inside the mth cluster. An example of the power delay profile of the S-V model is shown in Figure 3.3.

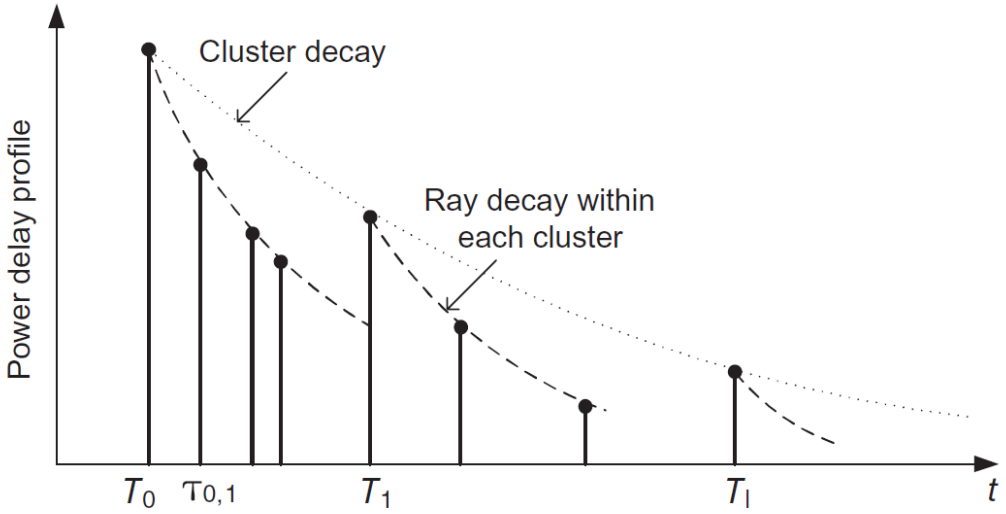

Fig. 3.3 S-V model power delay profile. Source Zekavat and Buehrer [25]

3.4.2 Impulse signals

Now that the behaviour of the channel has been explained, it is time to investigate which are the best type of impulse signals to be used in UWB systems. In order to to properly design antennas and circuits, the choice of the impulse shape is of paramount importance because it determines the spectrum characteristic of the signal. There is actually a large number of possible shapes that can be used to fulfil the technical requirements, but the most common are the step pulse and the Gaussian impulse and its derivative. Hereafter these signals will be described in more detail.

The step pulse or rectangular monocycle pulse is described in the time domain by the following equation

$$x(t) = \frac{1}{T_p}[U(t) - U(t - T_p] \tag{3.7}$$

where $U(t)$ is the unit step function and T_p is the width of the pulse. The parameter T_p can be used to tune the bandwidth of the signal and, in the case of UWB, it will be in the order of nanoseconds. This is clearly visible looking at the expression of the Fourier transform of the signal:

$$X(f) = \mathscr{F}[x(t)] = \frac{\sin(T_p \pi f)}{\pi f} \tag{3.8}$$

An example of rectangular monocycle pulse is shown in Figure 3.4. The representation of the signal in the frequency domain reveals the presence of a high Direct Current (DC) component. Typically, antennas are inefficient at DC and this is why this type of signal is not used in real applications. [5, 16]

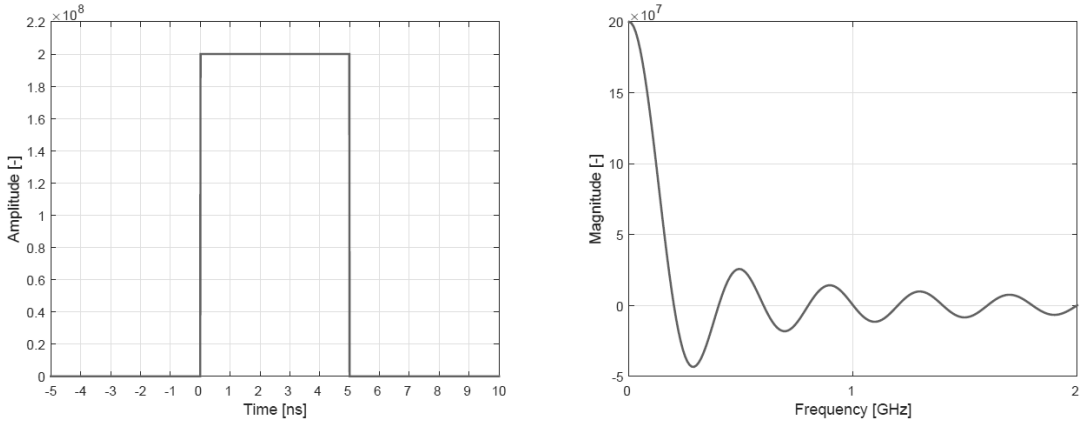

Fig. 3.4 Rectangular moncycle pulse in time and frequency domain

One of the most used signal shape in UWB systems is the Gaussian pulse and its time-derivatives [16]. The basic Gaussian pulse is described by the following expression:

$$x(t) = \frac{A}{\sqrt{2\pi\sigma^2}} e^{-\frac{t^2}{2\sigma^2}} \tag{3.9}$$

where A is the amplitude and σ is the standard deviation. Changing these two parameters is possible to control the gain and the width of the pulse. The Fourier transform is given by

$$X(f) = \mathscr{F}[x(t)] = A\mathrm{e}^{-\frac{(2\pi f\sigma)^2}{2}} \tag{3.10}$$

The shape of the Gaussian pulse in time and frequency domain is shown in Figure 3.5. Also in this case, there is a peak at zero frequency (high DC component) leading to the same problem related to the rectangular pulse.

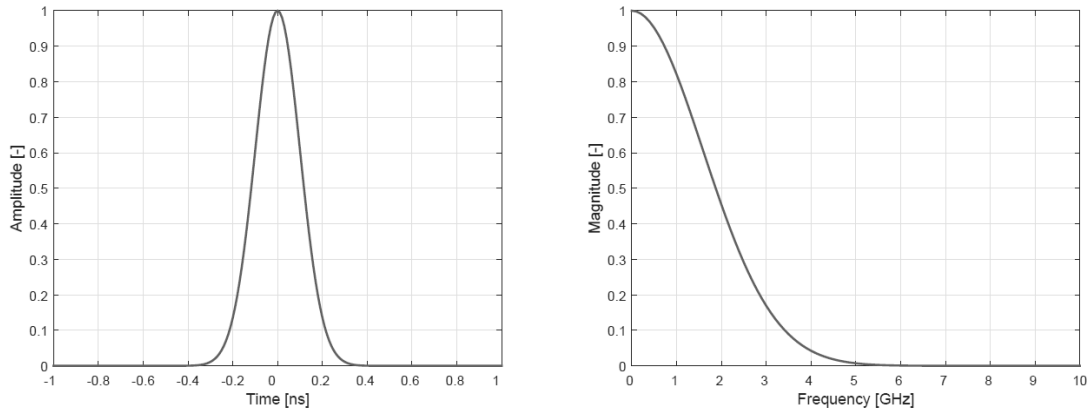

Fig. 3.5 Gaussian pulse in time and frequency domain

The expression of the nth time-derivative of a Gaussian pulse is given by the following recursive formula

$$x^{(n)}(t) = -\frac{n-1}{\sigma^2}p^{(n-2)}(t) - \frac{t}{\sigma^2}p^{(n-1)}(t) \tag{3.11}$$

and the relative Fourier transform is

$$X_n(f) = \mathscr{F}[x^{(n)(t)}] = (j2\pi f)^n A\mathrm{e}^{-\frac{(2\pi f\sigma)^2}{2}} \tag{3.12}$$

The behaviour of these pulses in frequency domain is plotted in Figure 3.6, with an increasing derivative order going from left to right. It is evident that even the first derivative eliminates the problem of the high radiated power at lower frequency. Moreover, higher order derivatives have higher central frequencies and a larger spectral bandwidth for the same pulse duration. This makes this type of pulses particularly suitable for UWB applications because it is easier to fit them in the mask imposed by FCC and EC regulations (Section 3.2). [16]

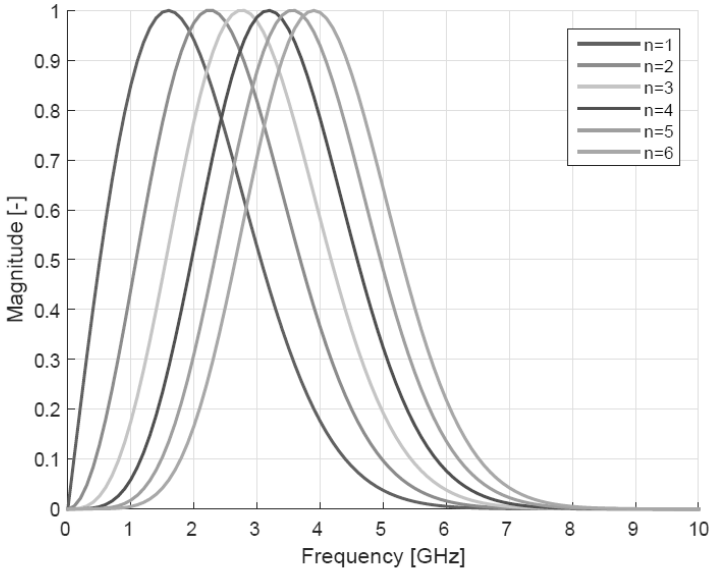

Fig. 3.6 Gaussian pulse time-derivative in frequency domain: the derivative order increase from left to right

3.4.3 Modulation topologies

A description of the UWB signal shapes and propagation properties has been given in the previous section. What is missing, in order to be able to transmit data, is signal modulation. Conversely from CW systems, in this case a carrier signal is not needed and so UWB systems are often called "base-band" or "impulse radio" systems. [16] Hereafter the most common modulating techniques are listed, along with a brief description of their functioning principles.

- *Pulse Position Modulation (PPM)*: with this technique, the value ("0" or "1") of the transmitted bits depends on the position of the corresponding pulses in the time domain. In this case the receiver is more complex, because it must measure the time position of the signal with high accuracy. [16] An example of PPM is shown in Figure 3.7
- *Pulse Amplitude Modulation (PAM)*: As shown in Figure 3.8 the high-amplitude pulses represent the logic value "1" and obviously the low-amplitude ones correspond to "0".
- *On-Off Keying (OOK)*: this method can be seen as a variation of PAM where the low-amplitude pulses have a value of the amplitude equal to zero. (Figure 3.9) The pulse is transmitted only when a "1" has to be sent and so the in this case the receiver must know the distribution of the time slots corresponding to the bits. [5, 16]

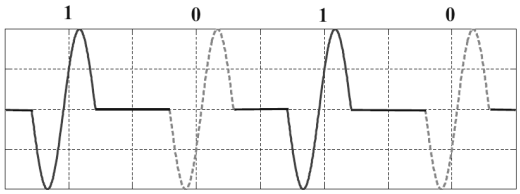

Fig. 3.7 Pulse Position Modulation

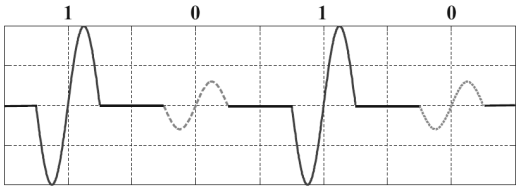

Fig. 3.8 Pulse Amplitude Modulation

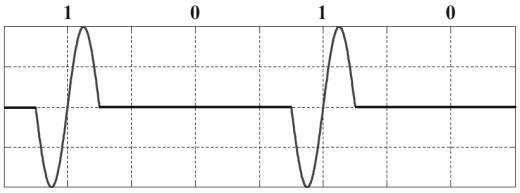

Fig. 3.9 On-Off keying

- *Bi-phase Shifting Keying (BPSK)*: differently from the other methods (mono-phase), BPSK distinguishes between ones and zeroes generating two pulses with opposite polarity. (Figure 3.10) With this technique the spectrum is smoother avoiding spikes caused by multi-pulse occurring periodically in PPM, PAM and OOK. Moreover, the overall power efficiency is significantly better when compared to OOK and PPM. [16]

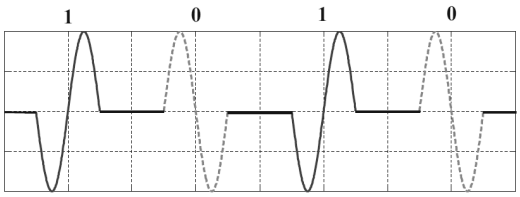

Fig. 3.10 Bi-phase Shifting Keying

3.4.4 Transmitter and receiver architecture

The circuitry in UWB devices, both transmitters and receivers, is typically less complex than the one used in CW systems. In UWB systems intermediate-frequency are not used and so complex components such as frequency synthesizers in the transmitter and mixers in the receiver become useless making UWB devices easier to design and less expensive. [16]

Figure 3.11 shows the basic components of a UWB transmitter. The oscillator is typically a cheap crystal oscillator and it determines the pulse repetition frequency (PRF) of the signal. The wanted pulse shape is produced by the pulse generator and then is modulated by a digital-controlled modulator using one of the techniques described in Section 3.4.3. The most important component is the pulse generator. As already mentioned, a bandwidth of 500 MHz or higher can be achieved only with very narrow pulses with a duration of few nanoseconds or lower and this can be challenging. The very first RF communication systems made use of spark-gap generators (Section 3.1) but they were abandoned because they caused excessive disturbances. Other circuits exploit Schottky barrier diodes and step recovery diodes, but in this case the spectral power distribution and the pulse duration are imposed by the fabrication process and cannot be changed at a later time. [16, 26] In modern devices, the need to produce adaptable signals that fit the regulation masks makes the use of CMOS radio frequency integrated circuits (RFICs) the best choice. [16]

The block diagram of a typical UWB receiver is shown in Figure 3.12. The basic circuitry of this device is composed by a low-noise amplifier (LNA), a correlator and a template pulse generator. The oscillator drives the pulse generator with PRF of the UWB system. In theory, to have the maximum signal to noise ratio, the shape produced by the pulse generator should

be the same of the received pulse signal. Once the noise is eliminated by the LNA, the template pulse is coherently correlated with the received and thus is converted in a base-band signal in a single stage.

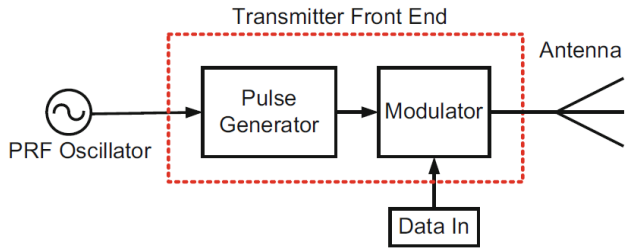

Fig. 3.11 UWB transmitter architecture

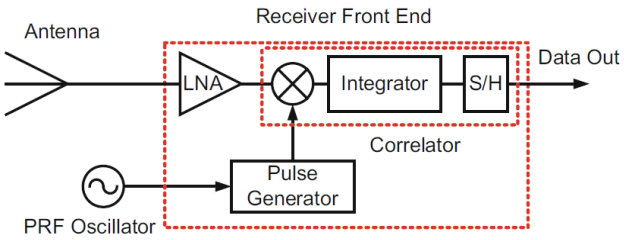

Fig. 3.12 UWB receiver architecture

3.5 Time-based ranging

Ranging is the ability of estimating the distance between a reference node and the target node. Hereafter, only the Time of Arrival (TOA) ranging method is discussed in detail. Among all the ranging techniques presented in Section 2.1.2, this is the most used in UWB systems and in particular is the one adopted by the Decawave TREK1000 evaluation kit used to perform the experimental measurements presented in Chapter 4. TOA is preferred to AOA of which implementation requires large and expensive antennas and also to RSS that present much poorer localization performance. [7] In general, time based ranging techniques better exploit the potentiality of the UWB technology. This can be seen from a mathematical point of view thanks to the Cramer-Rao inequality [7]:

$$\sqrt{Var(d)} \geq \frac{c}{2\sqrt{2}\pi\sqrt{SNR}\beta} \tag{3.13}$$

where the first member is the accuracy of the estimation of the distance d, c is the speed of light, SNR is the signal to noise ratio and β is the effective signal bandwidth.

The Equation 3.13 provides the formulation of the so called Cramer-Rao lower bound for a single path additive white Gaussian noise channel for time-based ranging. This is the maximum achievable localization accuracy given the characteristics of the signal. What is worth noticing is that the bandwidth appears at the denominator of the second member of the inequality, confirming that time-based UWB ranging systems can reach very high accuracy in distance measurements.

3.5.1 Time of arrival

For simplicity, let us consider a line-of-sight (LOS) condition, so the first path is the direct path of the signal, and a base-band signal which means that the Equation 3.3 of the CIR becomes $h(t) = \sum_{n=1}^{N} a_n \delta(t - \tau_n)$ (the phase parameter is neglected). Then, measuring the first path delay τ_0 it is possible to compute the distance d between the transmitter and the receiver as

$$d = c \cdot \tau_0 \tag{3.14}$$

where c is the speed of light.

For a narrow band system, given the transmitted signal $s(t)$, the received signal is expressed as

$$r(t) = As(t - T) + n(t) \tag{3.15}$$

where the parameters A and T are affected by all the multipath components and $n(t)$ is the white noise. The matched filtering estimator can only measure the optimal value of T which includes the effects of the reflected signals and so it is different from the first path delay. [25]

For a UWB system the received signal is given by the following expression:

$$r(t) = \sum_{n=1}^{N} a_n s(t - \tau_n) + n(t). \tag{3.16}$$

Unlike narrow band case, thanks to the multipath resolution of UWB, it is possible to estimate not only the first path delay τ_0, but also all the τ_n parameters.

3.5.2 Two-way ranging

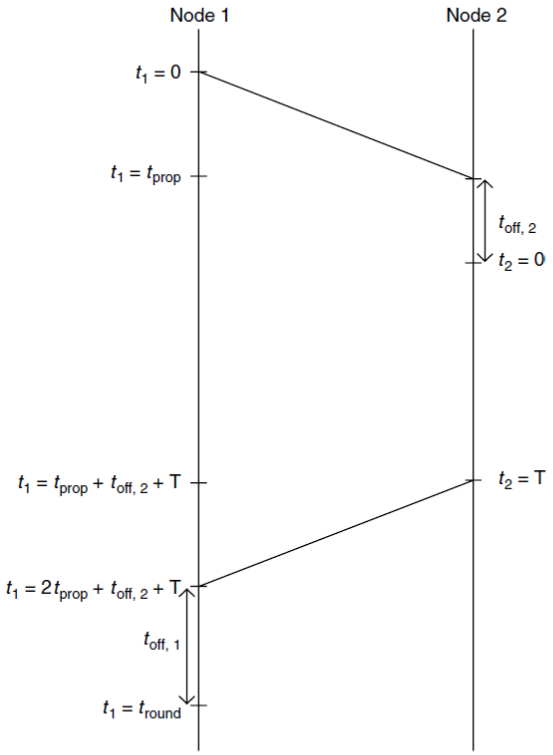

Fig. 3.13 TWR protocol. Source: Gezici et al. [7]

The Cramer-Rao lower bound, expressed by Equation 3.13, shows that the achievable accuracy under ideal condition is really high, thanks to the very high bandwidth of the pulse signals. This means that a precise clock synchronization between nodes becomes a crucial issue to obtain accurate distance estimation using TOA. [7]

One common solution to solve this problem is the so called Two-way ranging (TWR) protocol; its functioning principle is shown in Figure 3.13. The clocks of the two nodes are indicated with t_1 and t_2. When Node 2 receives the signal from Node 1, it set its clock to zero and, after a fixed time T, sends back a message to Node 1. Hence, the time of flight

t_{prop} can be computed as

$$t_{prop} = \frac{1}{2}(t_{round} - T - t_{off,1} - t_{off,2}) \tag{3.17}$$

where t_{round} is the total time measured by Node 1 from the first communication to the end of the measurement and $t_{off,1/2}$ denote the time errors committed in the detection of the signals. Note that the measurement is performed in two steps, thus it takes longer than a single TOA estimation but the elimination of a common timing reference is often a great advantage and it justifies the adoption of the TWR protocol.

3.6 Main sources of error

As demonstrated in Section 3.5, the theoretical ranging accuracy achievable with time-based ranging techniques is extremely high. This is true in a single user, LOS and single path situation, but in real world applications there are several issues that affect the accuracy of the localization system. The following list sums up the most critical sources of error in UWB positioning.

- *Multipath propagation*: TOA estimation is typically performed measuring the time shift of the template signal that produces the maximum correlation with the received signal. When dealing with single path channels, conventional correlation-based algorithms can be applied and the transmitted signal is used as optimal template signal. [7] Yet, in practical application, the channel is affected by multipath propagation and the template signal is given by the convolution of the transmitted signal and the channel impulse response (see Section 3.4.1). Thus, the correlation between the received signal and the transmit-waveform template is sub-optimal and, if applied to narrow-band signals, it often gives wrong TOA estimate because of the overlapping of the transmitted signal and the reflected ones. Thanks to the extremely short duration of the transmitted pulses, this phenomenon do not occur in UWB systems and the multipath components can be identified without using complex algorithms. [7]

- *Multiple access interference*: when different users are operating in the same environment, signals coming from different nodes can interfere. This leads to degraded TOA estimation and hence lower positioning accuracy. In order to overcome this problem, it is possible to use different techniques like time hopping codes with low cross-correlation properties and pulse-based polarity randomization. [7]

- *NLOS propagation*: the non-line of sight condition occurs when an obstacle is present between the transmitter and the receiver. In this case only the reflected component of the signal can reach the receiving node and so the measured TOA do not represent the direct signal path. Hence, the distance measurement is affected by a positive bias due to the larger distance travelled by the pulse. To obtain the optimal localization accuracy the typical approach is exclude NLOS measurements and so it is necessary to distinguish between LOS an NLOS components. Several techniques can be found in literature which are in most cases based on range statistics (LOS estimated range is Gaussian distributed with zero mean whereas NLOS are biased and non-Gaussian) or on channel characteristics, such as received signal power and features extracted from the power delay profile. [25] In other situations, it is impossible to use only LOS measurements and information on the environment can be used to compensate the NLOS error. [25]

- *High time resolution*: the extremely large bandwidth of UWB signals results in very high time resolution, which enables very accurate TOA estimation. However, it also poses some challenges in practical systems. First, clock jitter becomes an important factor in evaluating the accuracy of UWB positioning systems. Since UWB pulses have very short (subnanosecond) duration, clock accuracy and drifts in the target and the reference nodes affect the TOA estimates. Moreover, it is very impractical to sample the received signal at or above the Nyquist rate, which is typically on the order of tens of GHz. Therefore, TOA estimation schemes should make use of frame-rate or symbol-rate samples, which facilitate low-power designs.

3.7 Position estimation

Once the distances between the anchor nodes and the target node have been measured it is possible to compute the position of the target. This is basically a geometric problem. Let us consider for simplicity the 2D case; the location of the target can be can be computed as the intersection of the circles centered in the anchors' position (x_i, y_i) and having a radius equal to the measured distance d_i. Obviously, the minimum number of anchors needed to obtain a unique solution is equal to three. (Figure 3.14) The problem can be extended to the 3D localization, where the position of the target is given by the intersection of at least four spheres. From a mathematical point of view the unknown coordinates are computed as the solution of the system of equations of the circles (or spheres) which is overdetermined whenever the number of the anchor nodes is grater then the minimum. Moreover, in practical case it is very likely that the circles do not intersect all in the same point due to the presence

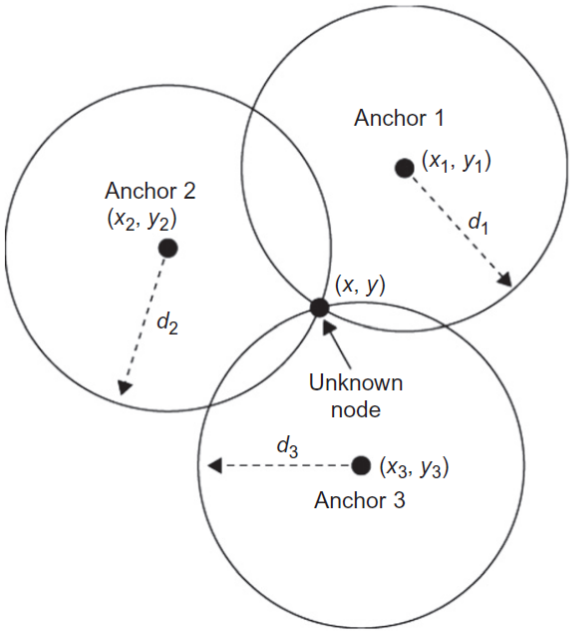

Fig. 3.14 2D positioning

of unavoidable errors in ranging measurements. So the typical approach to solve the problem is to use numerical algorithms that minimize the error function between the real and the estimated position. Between all the possible algorithms in Section 3.7.1 and 3.7.2 the Linear Least Squares (LLS) and the Gauss-Newton (G-N) are described in detail. The first is more suitable in the 2D case and is very undemanding from a computational point of view. The second has been chosen because it gives a very good trade-off between computation time and accuracy and it is easy to implement. These two algorithms are used and compared in the experiments presented in Chapter 4

3.7.1 Linearization

In 3D localization, the coordinates of the target node (x,y,z) are given by the solution of the following system of equation:

$$\begin{cases} (x-x_1)^2+(y-y_1)^2+(z-z_1)^2=d_1 \\ (x-x_2)^2+(y-y_2)^2+(z-z_2)^2=d_2 \\ (x-x_3)^2+(y-y_3)^2+(z-z_3)^2=d_3 \\ (x-x_4)^2+(y-y_4)^2+(z-z_4)^2=d_4 \end{cases} \tag{3.18}$$

where each equation is a sphere centered in the anchor position $p_i = [x_i, y_i, z_i]$ and having a radius d_i equal to the measured distance from the target node and the corresponding anchor. The equation of the sphere can be rewritten as

$$x^2 - 2xx_i + x_i^2 + y^2 - 2yy_i + y_i^2 + z^2 - 2zz_i + z_i^2 = d_i^2 \tag{3.19}$$

Now, subtracting, for example, the last equation from the other three it is possible to write the System 3.18 as

$$\begin{cases} -2[x(x_1 - x_4) + y(y_1 - y_4) + z(z_1 - z_4)] = d_1^2 - d_4^2 - \|p_1\|^2 + \|p_4\|^2 \\ -2[x(x_2 - x_4) + y(y_2 - y_4) + z(z_2 - z_4)] = d_2^2 - d_4^2 - \|p_2\|^2 + \|p_4\|^2 \\ -2[x(x_3 - x_4) + y(y_3 - y_4) + z(z_3 - z_4)] = d_3^2 - d_4^2 - \|p_3\|^2 + \|p_4\|^2 \\ (x - x_4)^2 + (y - y_4)^2 + (z - z_4) = d_4 \end{cases} \tag{3.20}$$

The system composed by the first three equation of 3.20 is a linear system that can by expressed by in matrix form ($\mathbf{A}\underline{x} = \mathbf{b}$), where the matrix A is

$$A = -2 \begin{vmatrix} (x_1 - x_4) & (y_1 - y_4) & (z_1 - z_4) \\ (x_2 - x_4) & (y_2 - y_4) & (z_2 - z_4) \\ (x_3 - x_4) & (y_3 - y_4) & (z_3 - z_4) \end{vmatrix}$$

and the matrix $\mathbf{b}$ is

$$b = \begin{vmatrix} d_1^2 - d_4^2 - \|p_1\|^2 + \|p_4\|^2 \\ d_2^2 - d_4^2 - \|p_2\|^2 + \|p_4\|^2 \\ d_3^2 - d_4^2 - \|p_3\|^2 + \|p_4\|^2 \end{vmatrix}$$

To find the position of the target node, that is the vector $\underline{x} = [x, y, z]$, it is now possible to apply the well known linear least squares (LLS) algorithm:

$$\underline{x} = (\mathbf{A}^T \mathbf{A})^{-1} \mathbf{b} \tag{3.21}$$

The algorithm can be easily extended to the case of m(>4) anchors just picking one of the m equations and subtract it to the remaining $m - 1$. In this way the result is a overdetermined system of $m - 1$ linear equations and the best approximating solution can be found applying the LLS algorithm as shown before. This method is very convenient from a point of view of the computational cost. Nevertheless, the matrix $\mathbf{A}$, which depend on the positioning of the

anchor nodes, can be ill-conditioned or even singular leading to poor results or unsolvable systems.

3.7.2 Gauss-Newton method

As known, the Gauss-Newton method is an iterative process used to solve a non-linear least-squares approximation problem. The wanted solution is the one that minimize the sum S of the squares of the residuals:

$$S = \sum_{i=1}^{m} r_i^2 \tag{3.22}$$

In the 3D localization problem, if m is the number of anchors, the previous sum has m addenda and the ith residual can be written as a function of the coordinates of the target node:

$$r_i = d_i - \sqrt{(x-x_i)^2 + (y-y_i)^2 + (z-z_i)^2} \tag{3.23}$$

Let us call $\underline{x} = [x,y,z]^T$ the vector of the coordinates of the target node, $p_i = [x_i, y_i, z_i]^T$ the position of the ith anchor and d_i the distance between the two nodes. At each step of the iteration, starting from an initial guess $\underline{x_0}$ for the position of the target node, the algorithm return a value $\underline{x_{k+1}}$ that minimize the sum of the residual and is given by the following formula:

$$\underline{x_{k+1}} = \underline{x_k} - (\mathbf{J}^T\mathbf{J})^{-1}\mathbf{J}^T\mathbf{r}(\underline{x_k}) \tag{3.24}$$

where $\mathbf{r}$ is the vector function of the residuals and $\mathbf{J}$ is its Jacobian matrix which, at the $k-th$ step, has the following expression:

$$\mathbf{J} = -\begin{bmatrix} \frac{(x_k-x_1)}{\sqrt{(x_k-x_1)^2+(y_k-y_1)^2+(z_k-z_1)^2}} & \frac{(y_k-y_1)}{\sqrt{(x_k-x_1)^2+(y_k-y_1)^2+(z_k-z_1)^2}} & \frac{(z_k-z_1)}{\sqrt{(x_k-x_1)^2+(y_k-y_1)^2+(z_k-z_1)^2}} \\ \vdots & \vdots & \vdots \\ \frac{(x_k-x_m)}{\sqrt{(x_k-x_m)^2+(y_k-y_m)^2+(z_k-z_m)^2}} & \frac{(y_k-y_m)}{\sqrt{(x_k-x_m)^2+(y_k-y_m)^2+(z_k-z_m)^2}} & \frac{(z_k-z_m)}{\sqrt{(x_k-x_m)^2+(y_k-y_m)^2+(z_k-z_m)^2}} \end{bmatrix}$$

The G-N algorithm quits the iteration when the error is lower than the preset tolerance or after a maximum number of steps that is chosen by the user.

This method usually gives good results in terms computation time and accuracy, but some convergence problems may occur if the starting point $\underline{x_0}$ is not set properly. [26]

3.8 Anchors' positioning

The most common UWB localization systems are anchor-based that means that they exploit the prior knowledge of the position some nodes (anchors) in order to localize the target node. Thus, beside the ranging errors, another fundamental factor that influence the localization accuracy is the spacial deployment of the anchors. Some positioning algorithms are more sensitive then others, but unfavourable distribution of the sensors can always induce singularities and low precision in position estimation. To minimize the localization error in the working area, different solutions have been proposed to compute the best anchors layout for example heuristic search methods, acute triangular-based deployment, adaptive beacon placement, and optimal placement solutions via the maxL–minE algorithm. [25] Yang and Scheuing [24] propose a more theoretical approach in which they demonstrate that uniform angular arrays (regular polygons and solid shapes) are possible optimal solution for the positioning of the sensors. Moreover, when a large number of anchor nodes is available, it has been observed that a smart choice of a subgroup of sensors gives better result than using them all. The strategies to perform such selection include joint clustering technique, entropy-based information gain and convex hull selection, see [25] for more detail.

Anyway, these techniques are suitable when the anchors are considered to be fixed and this is the case of almost all UWB localization systems. In our case of study, instead, UWB sensors are mounted on drones whose position is known thanks to GPS. This means that the anchors are free to move and their positioning will be dynamic, permitting to avoid some of the common limitations of systems with static sensors, but introducing new challenges. It is obvious that, in this case, the working area is no more limited and the problem of finding optimal subgroups of anchors turns into finding the best deployment in order to maximize the visibility among sensors. Moreover, because of the movement of the drones and of the rover that we want to track, the positioning algorithm will have to take in to account the trajectory and the speed of the robots to obtain the beast localization accuracy. An interesting work on dynamic anchors positioning, that can be a starting point for future developments of our system, have been carried out by Bahr and Leonard [2]. In their paper the authors aim to track an underwater autonomous vehicle using two or more floating robots that equipped with GPS receivers. The proposed algorithm generate the path for the surface vehicles in order to minimize the trilateration error taking into account the uncertainties in the localization of the anchors.

Chapter 4

Experimental analysis

The goal of the experimental analysis that was carried out was to estimate the precision in the relative localization of the rover. To do that, we chose a set of commercially available UWB sensors and we performed some ranging measurements both LOS and NLOS. We placed the sensors at difference distances and we collected around 450 samples for each phase. The accuracy and the precision were computed for each distance. Moreover, we had at our disposal some data, deriving from other experiments, in which the position of a drone, hovering in a fixed location, was measured using a standard GPS and a dual frequency GPS. All this information was used to make a numerical analysis considering a static situation in which the four drones were flying at fixed positions and the rover could be placed in a different location but was not moving. To perform these computations, both the range measurements and the position of the anchors (drones) were modelled as normally distributed random variables. In order to verify this hypothesis, we carried out some positioning measurements too. We mounted the four anchors on four tripods and we built a grid of 32 points placed inside and outside the convex area determined by the anchors' position. For each point we took about 450 measurements and we computed the standard deviation in the plane and in the space. The same arrangement was simulated under the assumption of normally distributed ranging measurements and the results have been compared with the experimental ones.

4.1 Instrumentation

4.1.1 DecaWave TREK1000

For this experiment we chose the TREK1000 evaluation kit from DeacWave. As demonstrated in [19], this UWB positioning system has the best performance compared with other systems available on the market. Each TREK100 kit contains four EVB1000 units that can operate as

anchors or tags. The boards are equipped with DecaWave's DW1000 IEEE802.15.4-2011 UWB compliant wireless transceiver IC(Table), STM32F105 ARM Cortex M3 processor, USB interface, LCD display and off-board antenna. The system has an accuracy of ±10 cm using two-way ranging time-of-flight technique. The positioning accuracy estimated by the manufacturer is ±30 cm for a moving tag and the maximum measurable distance in LOS condition is about 300 m. The EVB1000 boards have different working modes that can be configured using the dip-switches. It is possible to choose between two channels (2 and 5), which have two different central frequencies (3.99 GHz and 6.48 GHz), and two data rates 110 kbps or 6.8 Mbps. The default setting (3.99 GHz and 110 kbps) has been used for all the measurements. This configuration is suggested for long distance ranging and it guarantees an update rate of 3.5 Hz confirmed by experimental tests. The TREK1000 kit is also supplied with a software that allow to save the acquired data and perform 2D localization, if three anchors are in the same plane. Since we wanted to compute the 3D position of the tag and we didn't want any limitation in the anchors' configuration, the software was only used to collect the ranging measurements.

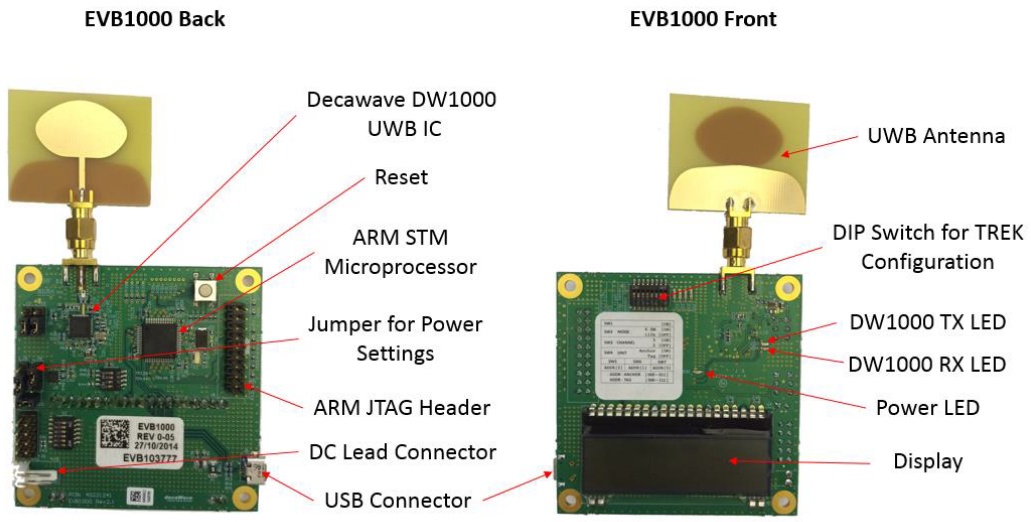

Fig. 4.1 Back and front views of EVB1000

Table 4.1 TREK1000 technical specs

Board Dimensions	120x70 mm (including external antenna)
Weight	39 grams
Operating Band	3.5-6.5GHz 6 Channels (500 MHz wide). U.S. FCC mask compliant.
Center Frequency	2 channels: Ch2: 3993.6 MHz, Ch5:6489.6 MHz
Power spectral density	-41.3 dBm/MHz max
Antenna	External: WB002 Omni-directional Planar Antenna
Ranging Techniques	Pulsed Two-Way Time-of-Flight defined as TWR (Two-Way Ranging)
Max Range	LOS: 290 m
Ranging precision	10 cm
Localization Technique	RTL software provided by manufacturer (see user manual for more information)
Network Protocols	TDMA
Max Positioning update rate (3 anchors, 1 tag)	3.57 Hz / 10 Hz (Depending on the operating mode)

4.1.2 Laser distance meter

Fig. 4.2 Leica DISTO X3

Table 4.2 Laser distance meter technical specs

Accuracy with favourable conditions	1 mm / 0.04"
Accuracy with unfavourable conditions	2 mm / 0.08"
Range with favourable conditions	0.05 - 150m / 0.16 - 500ft
Range with unfavourable conditions	0.05 - 80m / 0.16 - 260ft
Smallest unit displayed	0.1 mm / 1/32 in
X-Range Power Technology	yes
Laser class	2
Laser type	635 nm, <1 mW

4.1.3 Drone

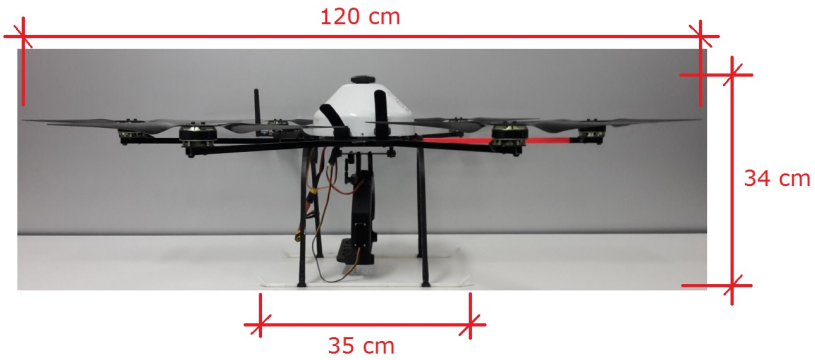

Fig. 4.3 Drone dimensions

Table 4.3 Drone technical specifications

Configuration	Esacopter with complanar rotors
Flight controller	Pixhawk 4
GPS/Compass module	3DR uBlox GPS
Base weight incl. batteries	3100 g
Max. payload	700 g
Drive	6 brushless motors (with 15" propellers)
Dimensions	Max diameter: 1200 mm Height: 340 mm
Flight time	15 min
Range	Electronically limited depending on the working scenario
Altitude	Electronically limited at 150 m
Operating temperature range	0/40°C
Recommended max. Wind speed	Up to 4 m/s
Max. horizontal speed	5 m/s
Max. vertical speed	-3/+5 m/s

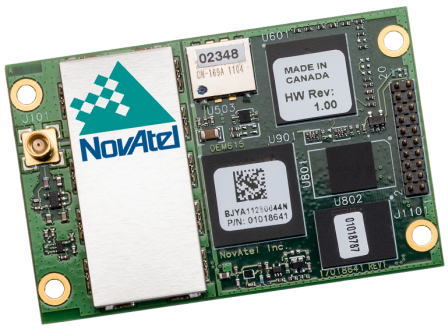

Fig. 4.4 Dual frequency GPS OEM615 NovAtel

Table 4.4 GPS OEM615 technical specs

System Type	Board	
General Info	Length (mm)	71.00
	Width/Diameter (mm)	46.00
	Height (mm)	11.00
	Weight (g)	24.00
	Typical Power Consumption (W)	1.00
Constellation	GPS	
	GLONASS	
	Galileo	
	BeiDou	
Tracking	Max Num of Frequency	Dual
	SBAS	
	QZSS	
Number of Com Ports	CAN Bus	2
	LVTTL	3
	USB Device	1
Performance	Accuracy	(RMS)
	Single Point L1	1.5m
	Single Point L1/L2	1.2m
	SBAS	0.6m
	DGPS	0.4m
	NovAtel CORRECT™ RT-2®	1 cm + 1 ppm

4.2 Ranging measurements

4.2.1 Line of sight

The measurements in line of sight were performed in outdoor environments (Fig.4.5). The sensors were placed at a height of about 30 cm from the ground level and the reference distances were measured with a measuring tape. We performed 13 measurements at 5, 6, 7, 8, 9, 10, 20, 30, 40, 50, 70, 100 meters and for each step we recorded for about 2 minutes, at a frequency of 3.5 Hz, that equates to more or less 420 samples. The sensors were able to exchange some information for up to a maximum distance of 157 meters, but the we observed a significant amount of missed measurements for distances above 100 meters.

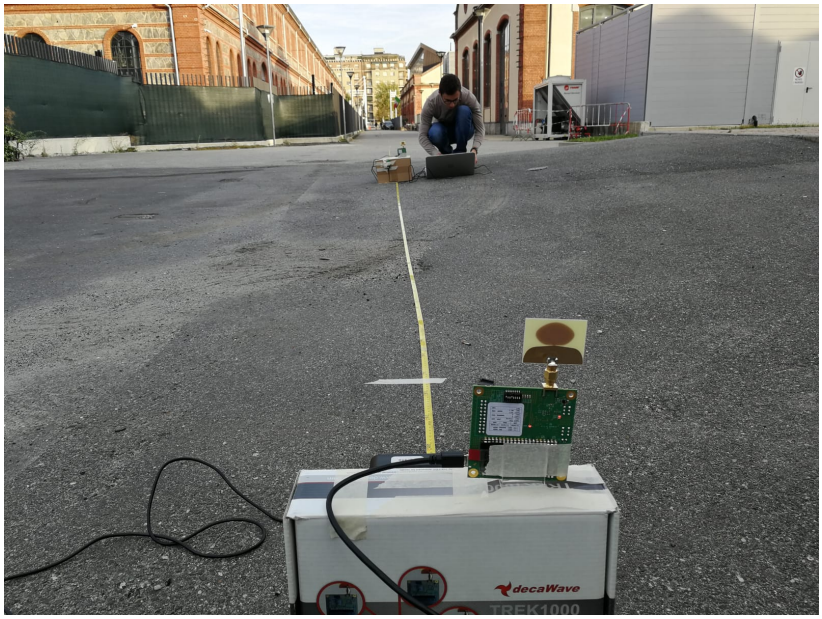

Fig. 4.5 Experimental setup for ranging LOS measures

The distribution of the error for each distance is shown in Figure 4.6. The real distance value, measured with the measuring tape, the mean value of the data acquired using UWB, the error, computed as the difference between the real distance and the mean, and the standard deviation are reported in Table 4.5. To verify if the measurements are actually normally distributed, the skewness and the kurtosis were computed. A normal distribution is characterized by a value of skewness of 0 and kurtosis equal to 3. In Table 4.6 we can see that the results are good enough to justify the assumption of normality with the exception of the ninth measurement (40 meters). This was probably caused by and accidental movement of the sensor before the end of the recording.

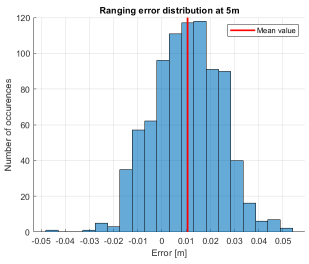

(a) Distance: 5 m

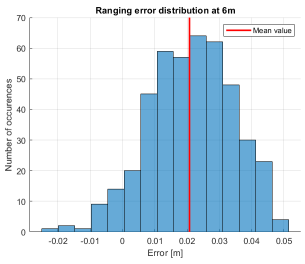

(b) Distance: 6 m

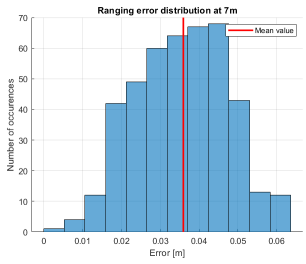

(c) Distance: 7 m

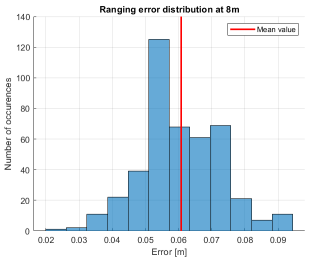

(d) Distance: 8 m

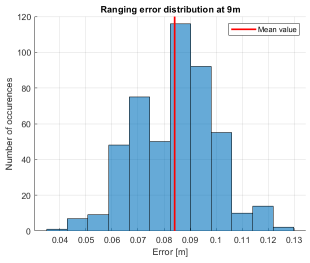

(e) Distance: 9 m

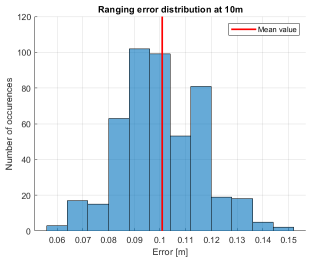

(f) Distance: 10 m

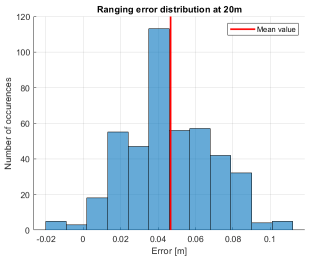

(g) Distance: 20 m

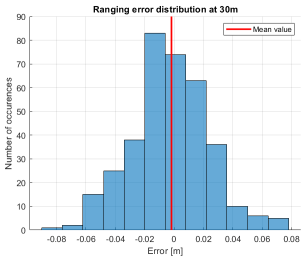

(h) Distance: 30 m

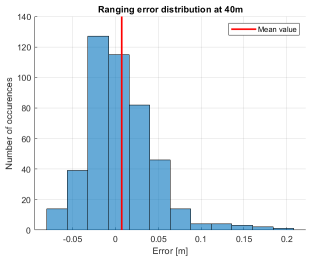

(i) Distance: 40 m

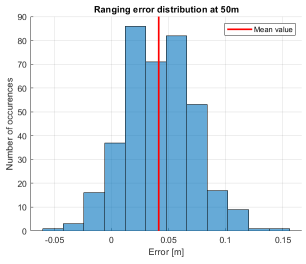

(j) Distance: 50 m

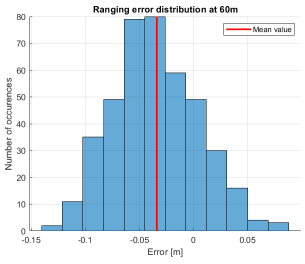

(k) Distance: 60 m

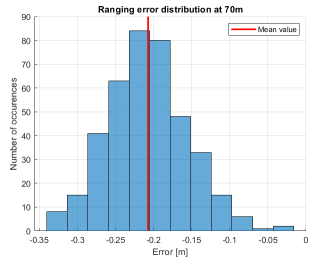

(l) Distance: 70 m

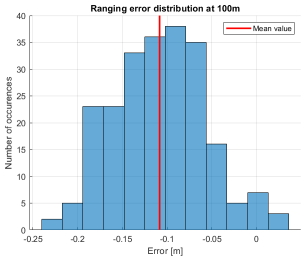

(m) Distance: 100 m

Fig. 4.6 Ranging error distribution at different distances in line of sight

Table 4.5 Experimental values LOS

	Real distance [m]	Mean value [m]	Error [m]	Standard deviation [m]
1	5,000	5,011	0,011	0,013
2	6,000	6,021	0,021	0,012
3	7,000	7,036	0,036	0,011
4	8,000	8,061	0,061	0,012
5	9,000	9,084	0,084	0,016
6	10,000	10,101	0,101	0,016
7	20,000	20,047	0,047	0,023
8	30,000	29,998	-0,002	0,027
9	40,000	40,007	0,007	0,040
10	50,000	50,041	0,041	0,030
11	60,000	59,966	-0,034	0,038
12	70,000	69,793	-0,207	0,053
13	100,000	99,892	-0,108	0,051

Table 4.6 Skweness and Kurtosis LOS

	Skewness	Kurtosis
1	-0,166	3,299
2	-0,218	3,099
3	-0,260	2,799
4	0,181	3,119
5	-0,003	2,795
6	0,041	2,890
7	0,006	2,922
8	0,061	3,161
9	1,022	5,789
10	0,214	3,407
11	0,201	2,752
12	0,280	3,297
13	0,186	2,663

4.2.2 Non-Line of sight

The experiment in non-line of sight was performed in an outdoor environment too, but, in this case, the two UWB sensors were separated by a brick parapet (Figure 4.7). One of the EVB1000 modules was kept at a fixed distance of 28 cm from the barrier, the other was moved at eight different positions. The reference measurements were collected with a laser distance meter to ensure high precision. The instrument was 15 cm from the wall, so the real distance between the two sensors is the measured one, plus the space between the first sensor and the parapet, plus the wall width (19 cm), plus 15 centimeters. The maximum measured distance was around 24 meters, significantly less than the LOS case.

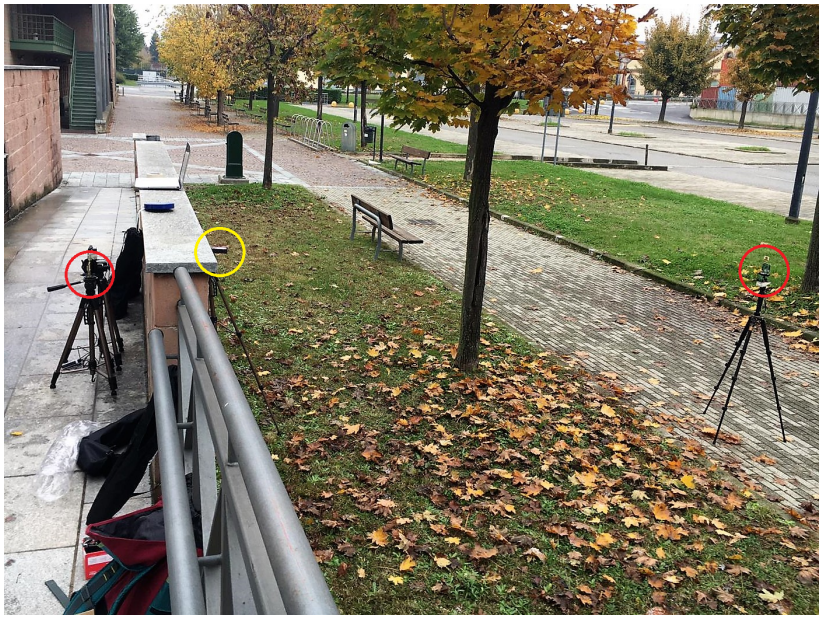

Fig. 4.7 Experimental setup for ranging NLOS measures: the two EVB1000 modules are highlighted in red, in yellow the laser distance meter

The plots in Figure 4.8 show the distribution of the error for each reference distance. All the numerical values are reported in Table 4.7 and Table 4.6. In this case the skweness and the kurtosis indicate that the error can be considered normally distributed too.

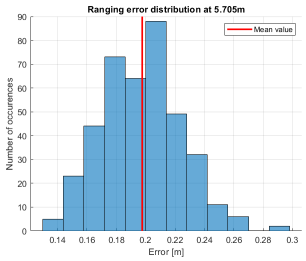

(a) Distance: 5 m

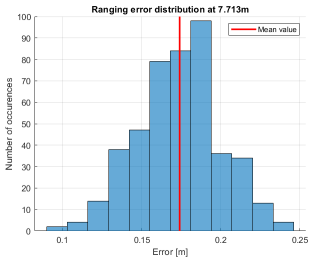

(b) Distance: 7 m

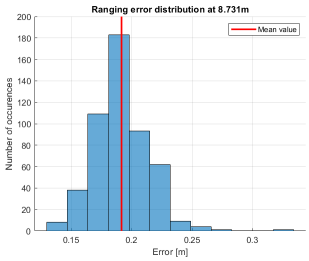

(c) Distance: 8 m

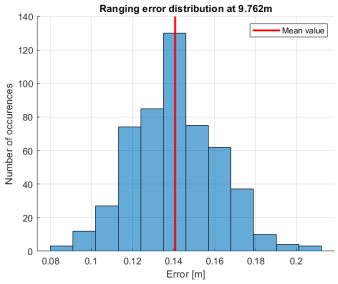

(d) Distance: 9 m

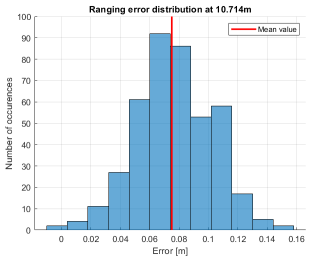

(e) Distance: 10 m

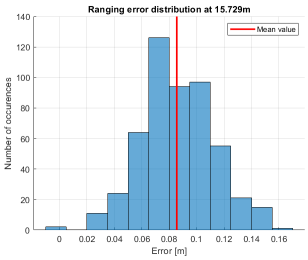

(f) Distance: 15 m

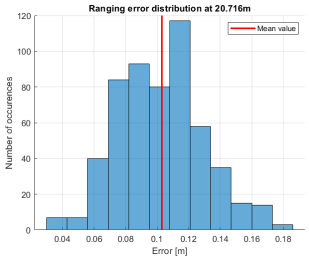

(g) Distance: 20 m

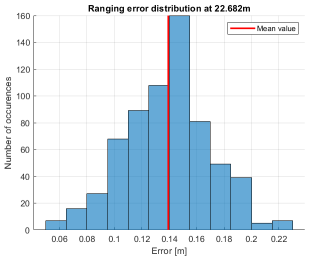

(h) Distance: 22 m

Fig. 4.8 Ranging error distribution at different distances in non-line of sight

Table 4.7 Experimental values NLOS

	Real distance [m]	Mean Value [m]	Error [m]	Standard deviation [m]
1	5,705	5,903	0,198	0,025
2	7,713	7,887	0,174	0,026
3	8,731	8,923	0,192	0,022
4	9,762	9,903	0,141	0,021
5	10,714	10,789	0,075	0,026
6	15,729	15,815	0,086	0,027
7	20,716	20,819	0,103	0,027
8	22,682	22,821	0,139	0,031

Table 4.8 Skweness and Kurtosis NLOS

	Skewness	Kurtosis
1	0,341	3,320
2	-0,087	2,772
3	0,625	5,779
4	0,147	2,961
5	-0,036	2,961
6	-0,024	2,953
7	0,245	2,986
8	0,023	2,861

4.2.3 Comparing LOS and NLOS

In Figure 4.9 the results of the ranging measurements are summed up using box-plots. It can be noticed that in from 0 to 22 meters the dispersion of the data in LOS and NLOS cases is comparable, even if it is slightly better in the first case as awaited. The values of the mean error, represented with purple lines in the plot, respect the theoretical expected behaviour that means an offset close to zero in LOS and a greater one in the presence of an obstacle, numerical values can be found in Table 4.9. However, looking at the single measurements it is evident that the error is significantly variable. This can be caused by signal reflection especially in LOS situation in which the sensors were placed very close to the ground.

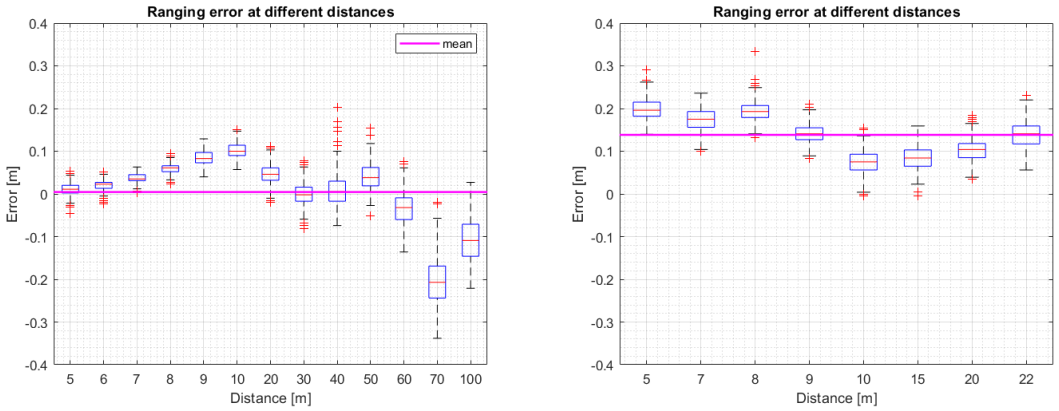

(a) LOS conditions

(b) NLOS conditions

Fig. 4.9 Ranging precision and accuracy LOS and NLOS. The boxplot shows the 25th and the 75th percentiles. The red crosses are the outliers

Table 4.9 Mean accuracy and precision LOS and NLOS

	Mean Error	**Mean Sigma**
LOS	0.004	0.026
NLOS	0.138	0.026

4.3 Positioning measurements

4.3.1 Drone hovering

One of the main source of error that affect the precision of the whole system is the uncertainty in the positioning of the anchors. In order to evaluate the localization precision of a drone

hovering in fixed position, some data deriving from another experiment carried out by the DIATI (Dipartimento di ingegneria dell'ambiente, del territorio e delle infrastrutture) lab was taken into account. The flight was executed with the drone described in Section 4.1.3 equipped with the OEM615 NovAtel dual frequency GPS module. The data is relative to a complete flight of the duration of about eleven minutes, but we took into account just the three minutes in which the drone was actually flying in a stationary position (Figure 4.10). The mean position and the standard deviation are reported in Table 4.10.

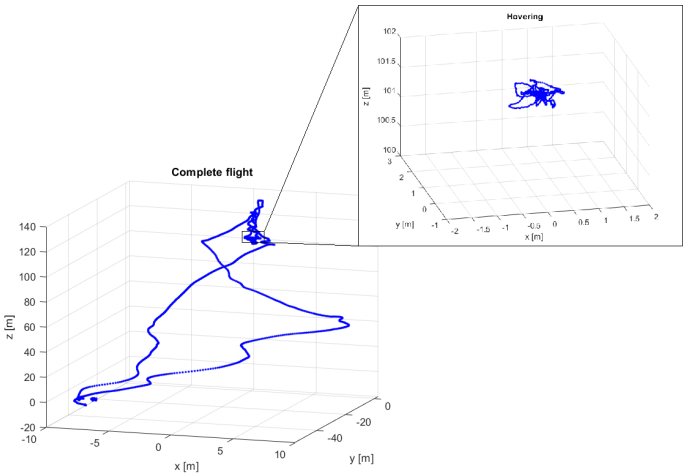

Fig. 4.10 Drone flight: the enlarged area shows the period selected as hovering condition

Table 4.10 Drone localization precision

	x [m]	y [m]	z [m]
Mean position	0,236	0,756	101,508
Standard deviation	0,215	0,333	0,024

4.3.2 Static positioning

To evaluate the positioning precision of the TREK1000 kit, we performed some static measurements. We built a squared grid of side 10 meters containing 36 points (one every 2 meters). The anchors were placed in 4 points at slightly different heights and avoiding symmetrical geometries in order to consider a general arrangement (Figure 4.11 and 4.12, Table 4.11). Hence, the tag was placed over each of the remaining 32 points and we collected the ranging measurements for about 2 minutes. The data was used to compute the position, the accuracy and the precision with two different algorithms: LLS and Gauss-Newton NLLS (see Section 3.7.1 and 3.7.2).

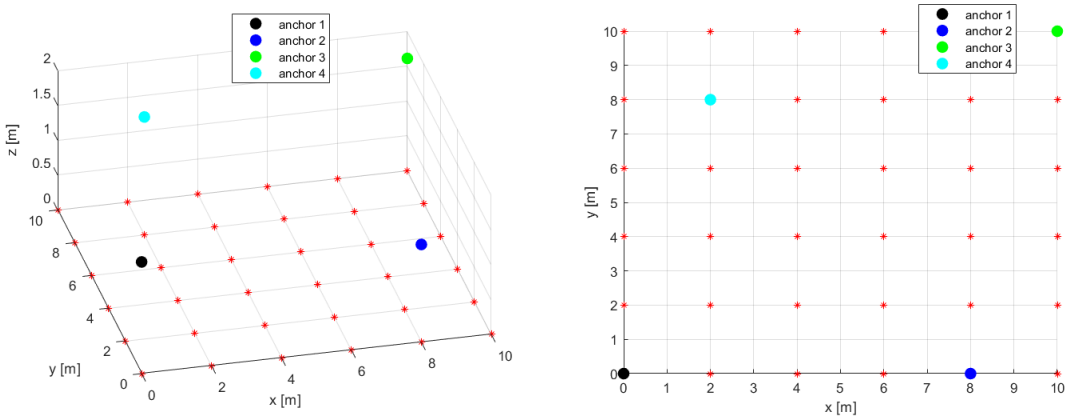

(a) (b)

Fig. 4.11 Position of the anchors and the grid points

Fig. 4.12 Static positioning experimental setup

Table 4.11 The anchors' position

	x [m]	y [m]	z [m]
Anchor 1	0,00	0,00	1,60
Anchor 2	8,00	0,00	1,40
Anchor 3	10,00	10,00	1,61
Anchor 4	2,00	8,00	1,69

In Figure 4.14, it is possible to see a comparison of the two algorithms. The used metrics are HDOP (horizontal dilution of precision) and PDOP (position dilution of precision) [11]:

$$HDOP = \frac{\sqrt{\sigma_x^2 + \sigma_y^2}}{\sigma_{ran} + \sigma anch} \tag{4.1}$$

$$PDOP = \frac{\sqrt{\sigma_x^2 + \sigma_y^2 + \sigma_z^2}}{\sigma_{ran} + \sigma anch} \tag{4.2}$$

where the numerators are the 2D and 3D precision respectively, σ_{ran} is the ranging precision and σ_{anch} is the precision in the positioning of the anchors. So, the two parameter are basically a measure of how much the positioning algorithm affects the localization accuracy. In this case the anchor position is known ($\sigma_{anch} = 0$), so the uncertainties that appear at the denominator of the HDOP and PDOP formulas are related only to the pseudo-range measurements. The value of σ_{ran} (equal to 0,0248 m) is computed as the mean of the standard deviation of all the range measurements of all 32 points. The value of the standard deviation in the points where the anchors are placed is set to σ_{ran} for graphical reasons.

It is well evident that the LLS gives much poorer results than NLLS. The value of HDOP in Figure 4.14a is not good (around 3.5) but acceptable, on the other hand the PDOP (Figure 4.14c) is greater than 100 almost everywhere which is an unfeasible result. This is due to the fact that, with this anchors' configuration, the matrix A, relative to the linearized system of equations (see Section 3.7.1, is ill-conditioned. In Figures 4.14b, 4.14d it is possible to see that the value of HDOP, obtained with NLLS algorithm, is very good (less than 1) in a large area, but the value of PDOP is poor being over 3 in the whole map with the exception of the points of the anchors where the value is not meaningful. Better results can be achieved with a proper configuration of the anchors, as discussed in the following paragraphs. All the numerical value can be found in Appendix A, Table A.1 and Table A.2.

Figure 4.15 and 4.16 show the mean position of all the 32 points. As expected the NLLS algorithm performs much better also in terms of accuracy. In the x-y plane the LLS still gives reasonable results, but along the z-axis the errors are unacceptable being in a range of more or less -11 meters and +14 meters. With the non-linear method, the results in the plane are excellent with the errors between a min value of 1,1 cm and a max of 12,3 cm. Along the 3-rd dimension there are some points that still present a low accuracy, but, inside the area delimited by the anchors, the result is pretty good.

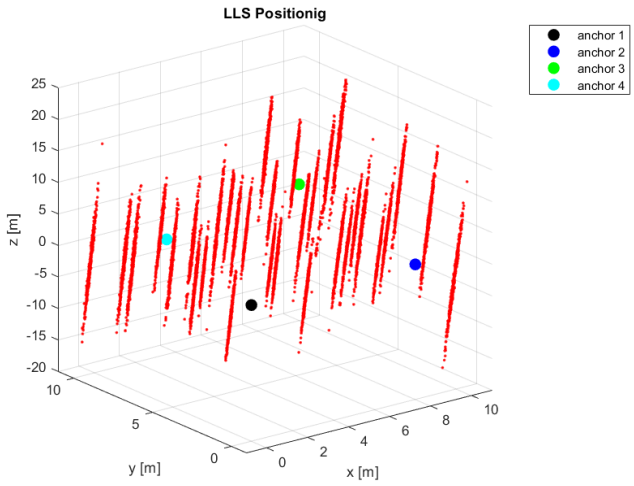

(a) LLS positioning

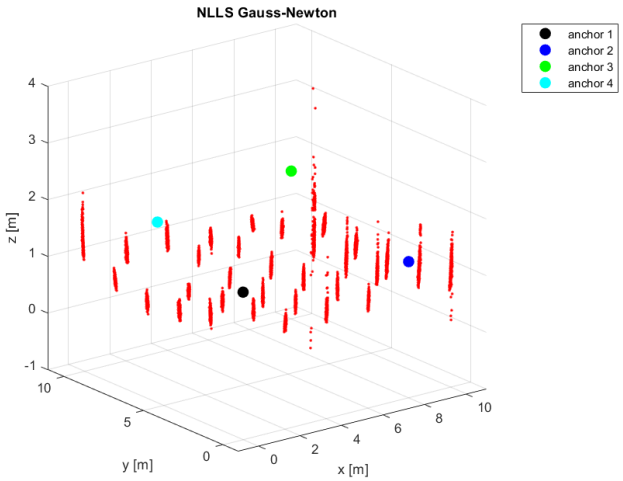

(b) NLLS positioning

Fig. 4.13 Positioning results

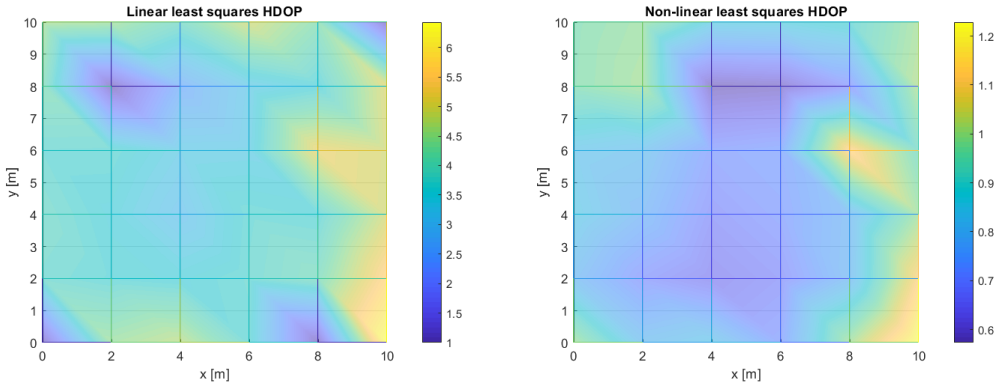

(a) LLS: HDOP

(b) NLLS: HDOP

(c) LLS: PDOP

(d) NLLS: PDOP

Fig. 4.14 Comparing HDOP and PDOP values obtained with LLS and NLLS algorithms

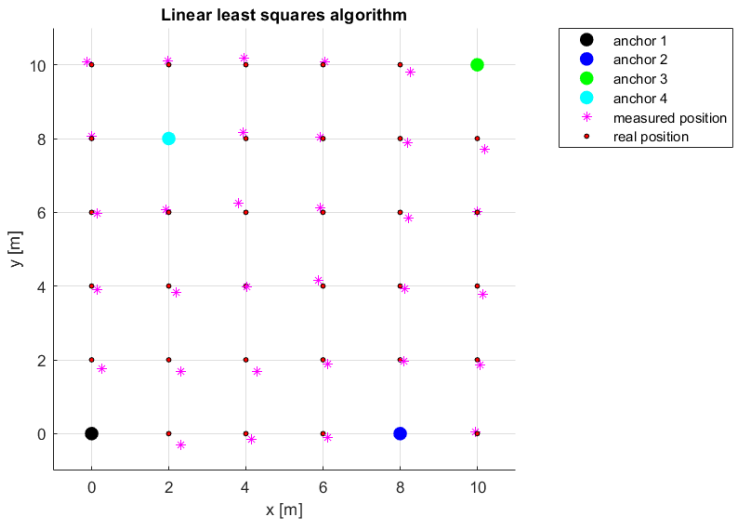

(a) LLS: mean position in x-y plane

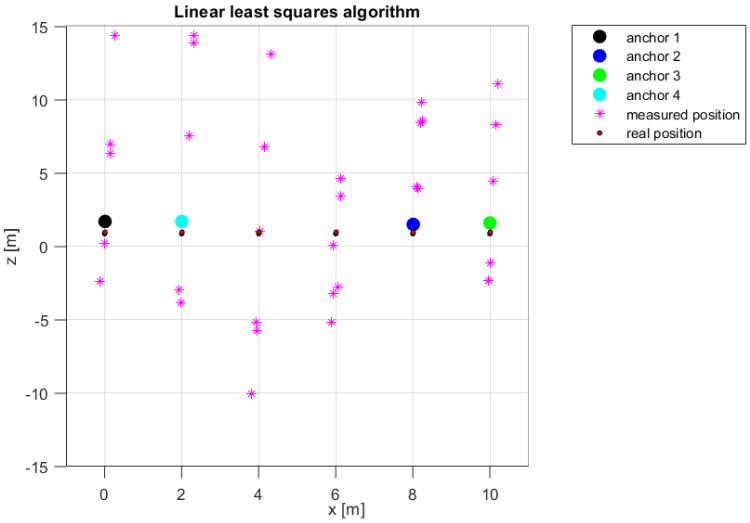

(b) LLS: mean position in x-z plane

Fig. 4.15 LLS positioning accuracy

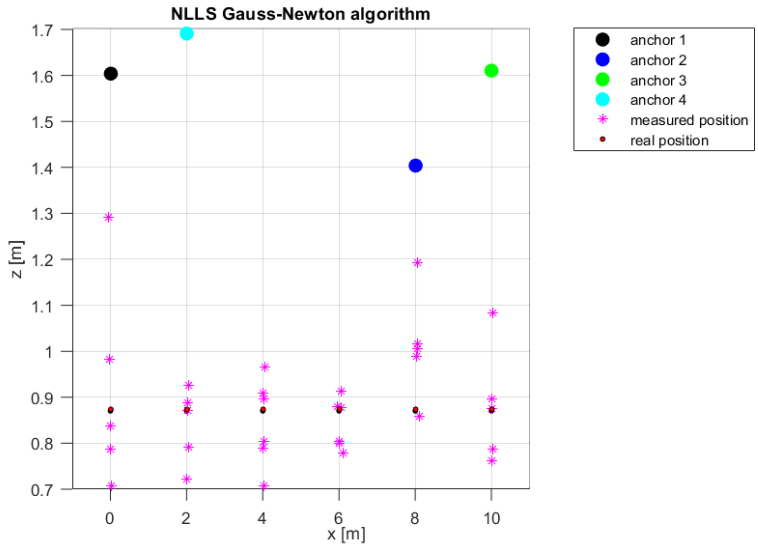

(a) NLLS: mean position in x-z plane

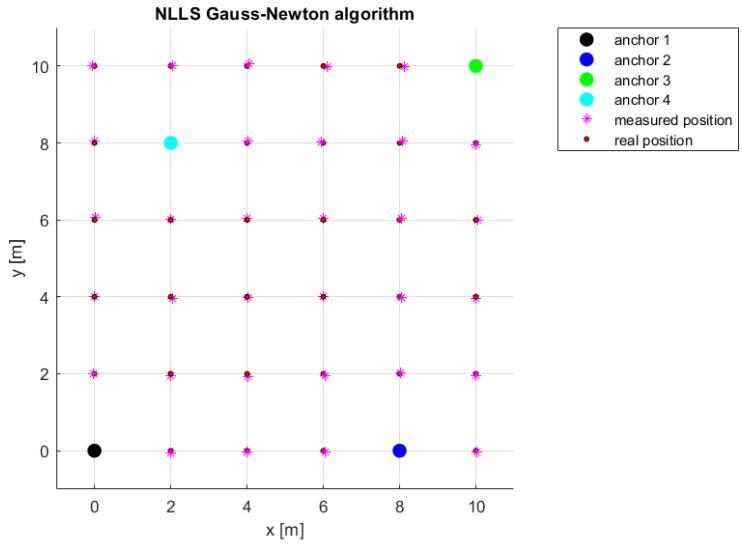

(b) NLLS: mean position in x-y plane

Fig. 4.16 NLLS positioning accuracy

4.3.3 Normality hypothesis validation

In order to make further considerations about the the performance of the system with different anchors' configuration, the measured quantities will be modelled as normally distributed random variables. To understand if this hypothesis is feasible, the same computations performed in the previous paragraph are repeated using normally distributed random variable instead of the measured distances. For each of the 36 points of the grid, we take into account 500 simulated positioning measurements. For each of the four anchors, the related 500 ranging measurements have a Gaussian distribution with the mean equal to the geometrical distance between the considered anchor and the tag plus an offset (4 cm) equal to the men value of the errors measured in the LOS ranging experiment; the standard deviation is put equal to the mean σ (2 cm) computed in the same experiment. The algorithm used to compute the position is the NLLS.

Comparing the color maps in Figure 4.17 and Figure 4.14b, 4.14d it is possible to verify that, excluding the point in position 8-6, the numerical result is very close to the experimental one. However, it is possible to see that the minimum value of HDOP is slightly better in the experimental case. On the other hand, analysing the cumulative distribution function of all the errors in the plane (Figure 4.18a), it is evident that, taking into account the whole grid, the numerical simulation gives better result: the slope of the blue curve is a little bit higher than the slope of the red one indicating a smaller variance and also the offset (value at 0,5 of probability) is more or less 2 cm smaller in the simulated case. On the contrary, in Figure 4.18b, the behaviour of the experimental curve is slightly better at least in the first part but shows the presence of a certain number of points for which the error is much greater than the mean.

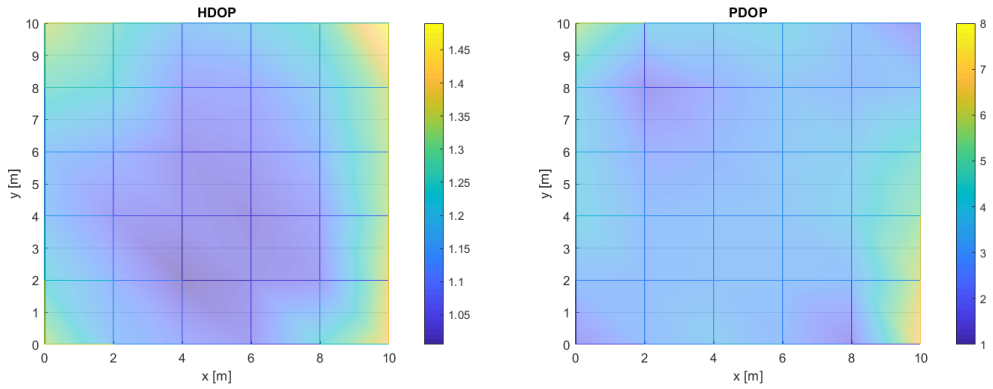

(a) Simulated HDOP (b) Simulated PDOP

Fig. 4.17 HDOP and PDOP color maps obtained under the hypothesis of normally distributed ranging measurements

Despite the described differences, the normality hypothesis on the distribution of the ranging measurements gives good results and it seems reasonable to use it to verify the performance of the whole system in different configurations. If one wants to use a more conservative analysis to be sure not to underestimate the error, it is always possible to assign higher values of the offset and the standard deviation to the modelled variables.

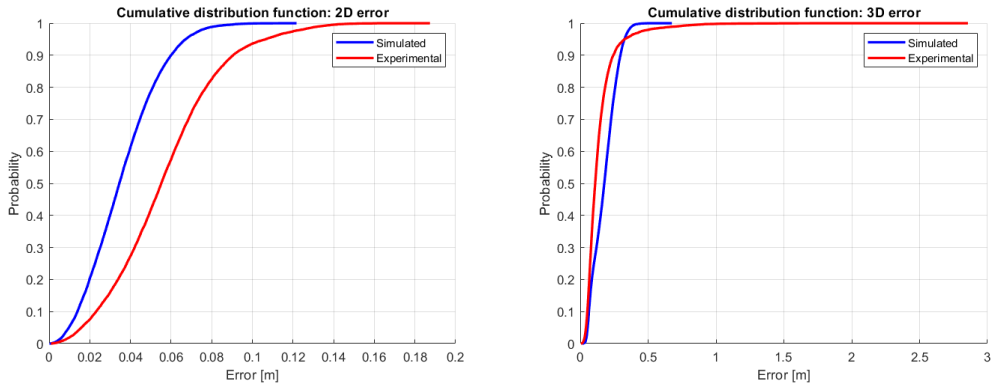

(a) CDF: 2D error

(b) CDF: 3D error

Fig. 4.18 Comparing simulation and positioning measures through the cumulative distribution functions

4.3.4 Anchors' positioning and global performance evaluation

The aim of the last part of the experiment is to evaluate through simulations the achievable precision of the system with an increasing number of anchors (from a minimum of three up to 6). A realistic situation is taken into account, where the drones are deployed at the vertexes of regular polygons inscribed in a circle with a radius of 14.14 m centered in the middle of the area of interest (Figure 4.19), as discussed in Section 3.8 this arrangement is optimal from the perspective of minimizing the 2D multilateration error. The flying height was set to 12 meters. The choice was made after several tries in order to obtain the best precision in the plane and in the space at the same time: higher altitudes increase the localization precision along the z-axis but gives poorer result in the x-y plane and vice versa. The position of 139 points deployed one every 2.5 m in the area of interest in a squared grid of side of 30 meters was computed. At total of 500 simulated measurements were considered for each point.

The values of the HDOP and PDOP were computed for each point in the same way as in Section 4.3.2 and the results are shown using color maps in Figure 4.20 and 4.21. As expected the points localized with the best precision are the ones in the central part of the map, the best obtained value with different number of anchors are reported in Table 4.12 and

the relative values of the standard deviation in the plane and in the space can be found in Table 4.13. In Figure 4.22 is possible to see how the localization performance of the system are changes with respect to the number of anchors. To quantify the improvement the values in Table 4.13 are divided by the worst value of the standard deviation (3 anchors case) and the normalized vale are plotted in Figure 4.23. It worth noticing that passing from three to six anchors there is a considerable increment of the precision of about 35% and 30% respectively in 2D and 3D case.

Table 4.12 HDOP and PDOP with an increasing number of anchors

	Min HDOP	**Max HDOP**	**Min PDOP**	**Max PDOP**
3 anchors	1.522	2.728	1.623	3.370
4 anchors	1.228	2.096	1.423	2.549
5 anchors	1.071	1.817	1.257	2.541
6 anchors	0.986	1.677	1.153	2.227

Table 4.13 Best values of the standard deviation with different number of anchors

	Min sigma_plane [m]	**Min sigma_spce[m]**
3 anchors	0.604	0.645
4 anchors	0.488	0.565
5 anchors	0.425	0.499
6 anchors	0.392	0.458

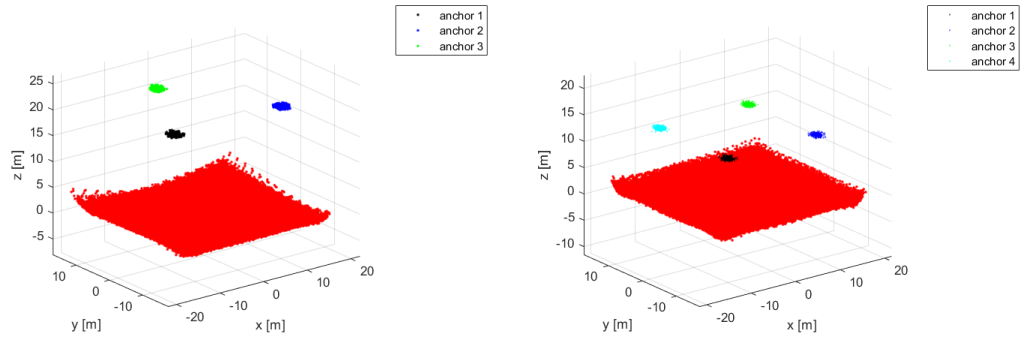

(a) 3 anchors configuration

(b) 4 anchors configuration

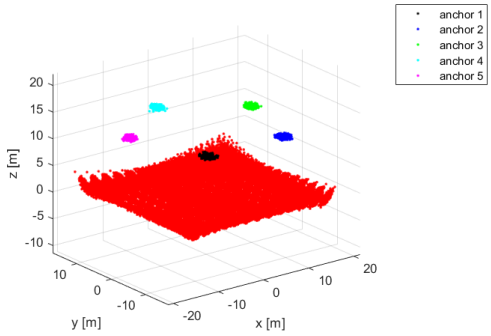

(c) 5 anchors configuration

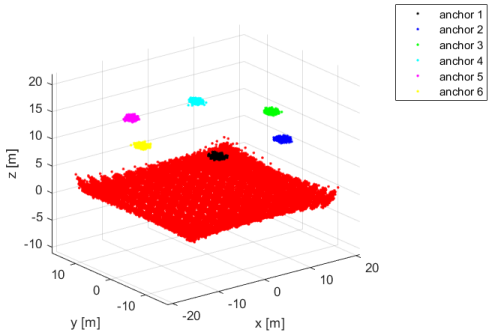

(d) 6 anchors configuration

Fig. 4.19 Anchors' configurations: different configurations with increasing number of anchors placed on the vertexes of regular polygons

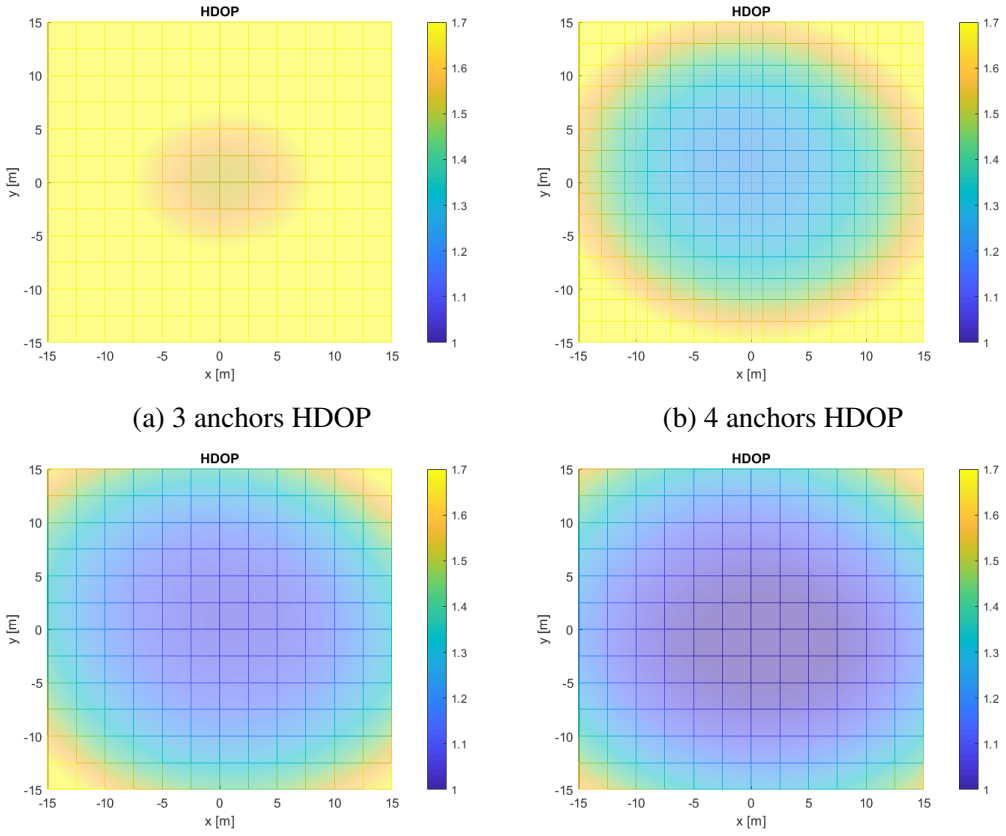

(a) 3 anchors HDOP

(b) 4 anchors HDOP

(c) 5 anchors HDOP

(d) 6 anchors HDOP

Fig. 4.20 HDOP values with an increasing number of anchors

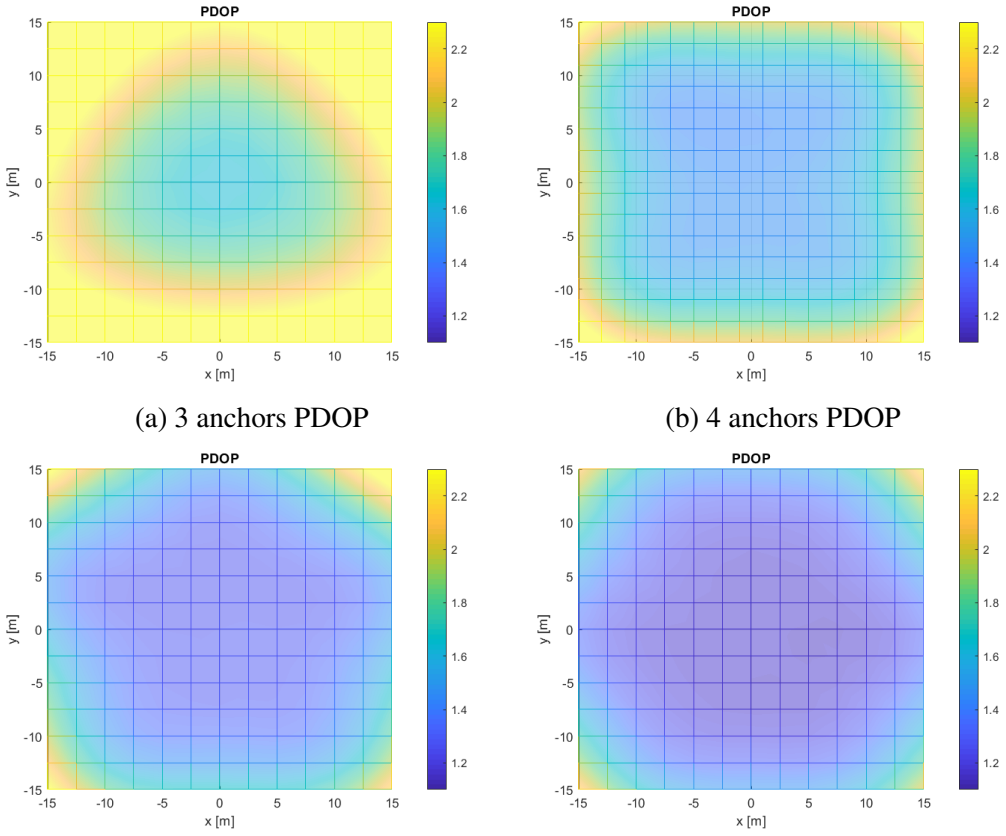

(a) 3 anchors PDOP

(b) 4 anchors PDOP

(c) 5 anchors PDOP

(d) 6 anchors PDOP

Fig. 4.21 PDOP values with an increasing number of anchors

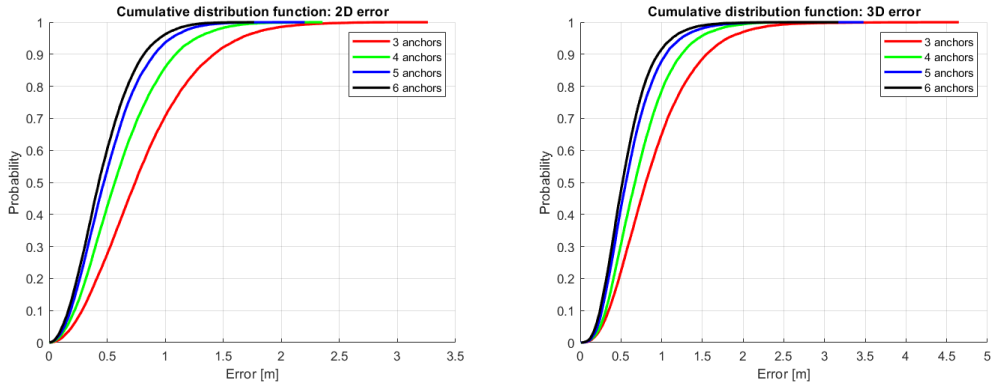

(a) CDF: 2D error (b) CDF: 3D error

Fig. 4.22 CDFs with an increasing number of anchors showing the error distribution in the whole area

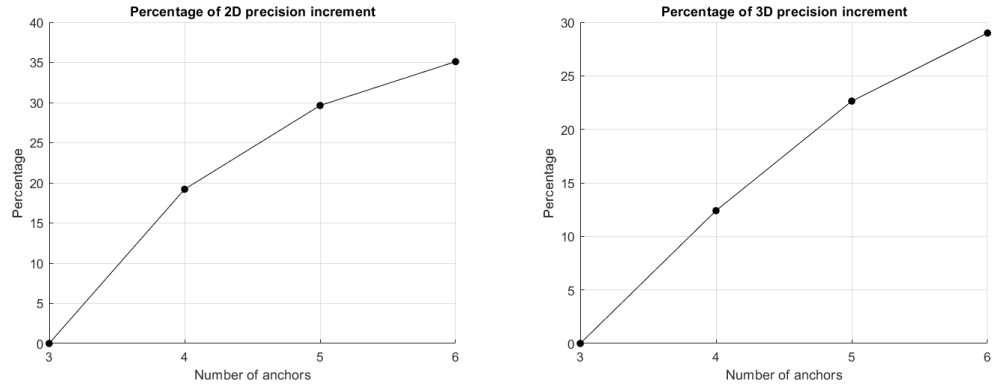

(a) Percentage of 2D precision increment (b) Percentage of 3D precision increment

Fig. 4.23 Precision increment with an increasing number of anchors

Chapter 5

Conclusions

This thesis proposes an innovative application of UWB technology for localization in robotic applications. The aim is to develop a positioning system for partially GPS-denied environments that does not need any kind of infrastructure (e.g. preexisting wireless network or landmarks). The proposed solution makes use of drones equipped with UWB sensors that act as mobile anchors. The innovation resides in the fact that the anchor nodes can be moved while the ground robot is operating, on the contrary, typical UWB localization systems rely on the knowledge of the precise position of fixed anchors. The possibility of dynamically place the drones can be exploited to constantly keep them in the best spacial configuration from the point of view of the minimization of the trilateration error. On the other hand, in order to avoid the degradation of the localization accuracy, new issues must be considered, for example the non-constant orientation of the antenna of the sensors, the uncertainties in the anchors position and the increased difficulty in NLOS signals identification. As the first phase of the design of the whole system, the experimental work that is proposed has two main goals: the first is to verify the performance of the TREK100 UWB evaluation kit, the second is to use the collected data to evaluate the precision of the system in relation with the uncertainties in the positioning of the anchors and their number.

The ranging experiment (Section4.2) confirms the centimeter precision in measuring the relative distance between two sensors both in LOS and NLOS condition. The precision expressed in terms of 95 percentile (two times the standard deviation) is always below the 11 cm with a mean value of 5,2 cm. Nevertheless, according to recorded measurements, the offset is not constant. In LOS conditions the difference between the maximum and the minimum offset is about 30 cm, while in NLOS it is about 11 cm despite the shorter measurable distance (22 m wrt 100 m in LOS). This is an undesirable behaviour because it makes it impossible to cancel the offset. Moreover, the maximum measured distance is 157 m against the expected maximum capability of 300 m.

With regards to positioning experiment (Section 4.3), it is possible to state that the LLS algorithm gives very poor results, in particular concerning the 3D localization in which the precision is of several meters. Using the G-N algorithm, instead, the results are much better confirming the precision of 30 cm declared by the manufacturer of the sensors. Indeed, among the 32 localized points only 4 have a precision above 30 cm and they are placed in unfavourable location (the edges of the grid). Also in this case the offset is not constant in particular along the vertical axis. The effectiveness of the G-N algorithm is confirmed by the computed values of the HDOP that stay below 1 in almost the whole map (Figure 4.14b), meaning that the algorithm attenuates the effects of the ranging errors. The values of the PODP, instead, are significantly worse being higher than 2,5, but this is due to the relative small distance between the anchors and the target node along the z-axis.

The simulation of a real world situation (Section 4.3.4) in LOS condition with an increasing number of anchors confirms that it is possible to obtain good localization precision. The possibility of moving the anchors allows to keep the target always in the barycenter of the drones' formation and so it is reasonable to take into account only the central part of the maps in Figure 4.20 and 4.21. In this area good values of the HDOP and PDOP can be reached with just 4 anchors. In this case, in the best situation, the precision in the plane is below 1 m. As expected the results further improve when the number of anchors increases: with six anchors the best values of HDOP and PDOP are 0.97 and 1.15 respectively and matching to a precision of 78 cm in the plane and 92 cm in 3D. Going from 3 to 6 anchors the improvement of the precision is about 35% in the plane and 30% in the space. Obviously in practical applications the choice of the number of anchors will be a compromise between the needed precision and the increasing cost and complexity of the system. The main limitations of this study are related to the fact that only LOS condition are considered and the both the drones and the rover are not moving.

Future works will include the building of a prototype of the system to validate the present work and perform more measurements in different environmental conditions. Moreover, the NOLS issue will be deepened trying different techniques to identify and mitigate the NLOS errors. The problem of tracking the ground vehicle while it is moving will be considered too and this will probably require the adoption of more complex algorithms (e.g. Kalman filter or Particle filter). Finally, the development of a control algorithm to properly place the anchors will be of paramount importance to obtain an effective localization system. Different strategies can be adopted reach this aim: beside using the optimal deployment from a geometrical point of view, other factors can be taken in to account such as maximizing the RSS, place at least some of the anchors in LOS (if possible) and use different flying height depending on the need to minimize the error in the plane or along the z-axis.

References

[1] Alarifi, A., Al-Salman, A., Alsaleh, M., Alnafessah, A., Al-Hadhrami, S., Al-Ammar, M. A., and Al-Khalifa, H. S. (2016). Ultra wideband indoor positioning technologies: Analysis and recent advances. *Sensors*, 16(5).

[2] Bahr, A. and Leonard, J. J. (2007). Minimizing trilateration errors in the presence of uncertain landmark positions. *3rd European Conference on Mobile Robots (ECMR)*, pages 48–53.

[3] Balamurugan, G., Valarmathi, J., and Naidu, V. P. S. (2016). Survey on uav navigation in gps denied environments. In *2016 International Conference on Signal Processing, Communication, Power and Embedded System (SCOPES)*, pages 198–204.

[4] Dardari, D., Luise, M., and Falletti, E. (2014). *Satellite and terrestrial radio positioning techniques: a signal processing perspective*. Elsevier Science, Saint Louis, MO.

[5] der Helm, S. V. (2018). On-board range-based relative localization for leader-follower flight of micro aerial vehicles. unpublished thesis.

[6] Di Benedetto, M.-G., Kaiser, T., , A., Oppermann, I., Politano, C., and , D. (2006). *Ultra-wideband Communication Systems: A Comprehensive Overview*. Hindawi Publishing Corporation.

[7] Gezici, S., Sahinoglu, Z., Kobayashi, H., and Poor, H. V. (2005). *Ultra Wideband Geolocation*, chapter 3, pages 43–75. John Wiley & Sons, Ltd.

[8] Guo, K., Qiu, Z., Miao, C., Zaini, A. H., Chen, C.-L., Meng, W., and Xie, L. (2016). Ultra-wideband-based localization for quadcopter navigation. *Unmanned Systems*, 04(01):23–34.

[9] Hegarty, C. J. (2017). *Springer Handbook of Global Navigation Satellite Systems*. Springer International Publishing, Cham.

[10] Hofmann-Wellenhof, B., Lichtenegger, H., and Wasle, E. (2008). *GNSS Global Navigation Satellite Systems: GPS, GLONASS, Galileo, and more*. Springer Vienna, Vienna.

[11] Kaplan, E. and Hegarty, C. (2017). *Understanding GPS/GNSS: Principles and Applications*. Artech House.

[12] Kia, S. S., Rounds, S., and Martinez, S. (2016). Cooperative localization for mobile agents: A recursive decentralized algorithm based on kalman-filter decoupling. *IEEE Control Systems Magazine*, 36(2):86–101.

[13] Kim, J. H., Kwon, J., and Seo, J. (2014). Multi-uav-based stereo vision system without gps for ground obstacle mapping to assist path planning of ugv. *Electronics Letters*, 50(20):1431–1432.

[14] Nehmzow, U. (2008). *Robotica Mobile*. Springer-Verlag Mailand. Italian editors A. Chella, R. Sorbello.

[15] Nekoogar, F. (2005). *In UltraWideband Communications Fundamentals and Applications*. Prentice Hall, San Ramon, California.

[16] Nguyen, C. and Miao, M. (2017). *Fundamentals of UWB Impulse Systems*, pages 7–24. Springer International Publishing, Cham.

[17] Nikookar, H. and Prasad, R. (2009). *Introduction to Ultra Wideband for Wireless Communications*. Springer, Dordrecht.

[18] Qiu, R. C., Liu, H., and Shen, X. (2005). Ultra-wideband for multiple access communications. *IEEE Communications Magazine*, 43(2):80–87.

[19] Ruiz, A. R. J. and Granja, F. S. (2017). Comparing ubisense, bespoon, and decawave uwb location systems: Indoor performance analysis. *IEEE Transactions on Instrumentation and Measurement*, 66(8):2106–2117.

[20] Singh, B., Sahoo, S. K., and Pradhan, S. R. (2012). Article: Performance evaluation of anchor-based range-based localization systems in wireless sensor networks. *International Journal of Computer Applications*, 52(17):24–29. Full text available.

[21] Sivaneri, V. O. and Gross, J. N. (2017). Ugv-to-uav cooperative ranging for robust navigation in gnss-challenged environments. *Aerospace Science and Technology*, 71:245 – 255.

[22] Wang, P., Liu, Z., Zhang, X., Xu, L., He, J., and Wan, Y. (2018). Wideband signal based near-field electromagnetic ranging for indoor localizatio. In *2018 International Conference on Advanced Control, Automation and Artificial Intelligence (ACAAI 2018)*. Atlantis Press.

[23] Xiang, J. and Hongyuan, Z. (2004). Sensor positioning in wireless ad-hoc sensor networks using multidimensional scaling. In *IEEE INFOCOM 2004*, volume 4, pages 2652–2661 vol.4.

[24] Yang, B. and Scheuing, J. (2005). Cramer-rao bound and optimum sensor array for source localization from time differences of arrival. In *Proceedings. (ICASSP '05). IEEE International Conference on Acoustics, Speech, and Signal Processing, 2005.*, volume 4, pages iv/961–iv/964 Vol. 4.

[25] Zekavat, R. and Buehrer, R. M. (2011). *Handbook of Position Location: Theory, Practice and Advances*. Wiley-IEEE Press, 1st edition.

[26] Zwick, T., Wiesbeck, W., Timmermann, J., and Adamiuk, G. (2013). *Ultra-wideband RF System Engineering*. EuMA High Frequency Technologies Series. Cambridge University Press.

Appendix A

Experimental data

Table A.1 LLS: accuracy, precision and DOP. Data relative to Paragraph 4.3.2

Point position	err_plane [m]	err_z [m]	sigma_plane [m]	sigma_space [m]	HDOP	PDOP
0-0 (Anchor 1)	0,000	0,000	0,025	0,025	1,000	1,000
0-2	0,367	13,421	0,094	3,152	3,780	127,003
0-4	0,168	6,026	0,096	3,590	3,879	144,651
0-6	0,143	5,413	0,092	3,347	3,708	134,892
0-8	0,065	-0,684	0,103	3,885	4,170	156,539
0-10	0,146	-3,276	0,114	4,348	4,605	175,210
2-0	0,438	12,916	0,111	3,532	4,471	142,315
2-2	0,438	13,456	0,090	2,906	3,611	117,120
2-4	0,252	6,622	0,087	2,971	3,510	119,716
2-6	0,113	-3,879	0,092	3,430	3,696	138,201
2-8 (Anchor 4)	0,000	0,000	0,025	0,025	1,000	1,000
2-10	0,101	-4,740	0,112	4,265	4,517	171,876
4-0	0,217	5,791	0,118	3,660	4,761	147,488
4-2	0,442	12,189	0,087	2,779	3,516	111,998
4-4	0,028	0,079	0,076	2,485	3,051	100,147
4-6	0,325	-10,921	0,082	2,860	3,288	115,231
4-8	0,181	-6,039	0,063	2,382	2,549	95,985
4-10	0,195	-6,593	0,098	3,716	3,929	149,742
6-0	0,166	3,651	0,091	2,863	3,679	115,355
6-2	0,154	2,468	0,093	2,891	3,733	116,508
6-4	0,190	-6,123	0,091	2,981	3,685	120,127
6-6	0,152	-4,106	0,082	2,939	3,318	118,427
6-8	0,077	-0,802	0,080	2,829	3,237	114,017
6-10	0,087	-3,633	0,122	4,518	4,935	182,067
8-0 (Anchor 2)	0,000	0,000	0,025	0,025	1,000	1,000
8-2	0,112	3,120	0,101	3,186	4,064	128,407
8-4	0,137	3,030	0,089	2,930	3,605	118,073
8-6	0,273	8,948	0,130	3,984	5,223	160,541
8-8	0,225	7,525	0,088	3,055	3,535	123,097
8-10	0,317	7,692	0,105	3,758	4,216	151,446
10-0	0,076	-3,267	0,160	4,920	6,428	198,259
10-2	0,159	3,497	0,139	4,449	5,616	179,268
10-4	0,263	7,365	0,123	4,120	4,948	166,040
10-6	0,029	-2,061	0,123	3,998	4,965	161,093
10-8	0,354	10,227	0,126	4,243	5,061	170,983
10-10 (Anchor 3)	0,000	0,000	0,025	0,025	1,000	1,000

Table A.2 NLLS: accuracy, precision and DOP. Data relative to Paragraph 4.3.2

Point position	err_plane [m]	err_z [m]	sigma_plane [m]	sigma_space [m]	HDOP	PDOP
0-0 (Anchor 1)	0,000	0,000	0,025	0,025	1,000	1,000
0-2	0,034	0,108	0,020	0,080	0,794	3,206
0-4	0,011	-0,086	0,021	0,072	0,850	2,899
0-6	0,076	-0,165	0,021	0,068	0,831	2,753
0-8	0,053	-0,033	0,024	0,071	0,961	2,865
0-10	0,057	0,422	0,024	0,183	0,958	7,387
2-0	0,048	0,013	0,020	0,056	0,808	2,245
2-2	0,043	-0,002	0,017	0,070	0,695	2,828
2-4	0,062	-0,080	0,019	0,065	0,778	2,630
2-6	0,014	-0,149	0,020	0,052	0,813	2,110
2-8 (Anchor 4)	0,000	0,000	0,025	0,025	1,000	1,000
2-10	0,054	0,055	0,025	0,089	0,989	3,574
4-0	0,045	0,036	0,021	0,120	0,837	4,840
4-2	0,073	-0,068	0,016	0,073	0,644	2,927
4-4	0,021	-0,165	0,017	0,081	0,678	3,281
4-6	0,037	-0,082	0,018	0,073	0,711	2,926
4-8	0,059	0,025	0,014	0,053	0,574	2,122
4-10	0,074	0,096	0,021	0,084	0,856	3,397
6-0	0,050	0,039	0,018	0,081	0,715	3,277
6-2	0,076	0,005	0,017	0,084	0,677	3,376
6-4	0,015	-0,068	0,018	0,087	0,713	3,496
6-6	0,046	-0,071	0,018	0,082	0,728	3,286
6-8	0,057	0,009	0,014	0,062	0,584	2,518
6-10	0,109	-0,091	0,021	0,071	0,863	2,841
8-0 (Anchor 2)	0,000	0,000	0,025	0,025	1,000	1,000
8-2	0,046	0,115	0,020	0,134	0,791	5,381
8-4	0,054	0,133	0,020	0,149	0,787	6,016
8-6	0,067	0,322	0,028	0,412	1,130	16,618
8-8	0,090	0,146	0,017	0,066	0,693	2,648
8-10	0,123	-0,012	0,022	0,052	0,894	2,103
10-0	0,035	0,210	0,030	0,207	1,228	8,338
10-2	0,059	0,001	0,028	0,189	1,115	7,608
10-4	0,036	-0,111	0,025	0,134	0,991	5,388
10-6	0,047	-0,084	0,023	0,087	0,932	3,501
10-8	0,062	0,025	0,025	0,079	1,016	3,181
10-10 (Anchor 3)	0,000	0,000	0,025	0,025	1,000	1,000

Table A.3 Simulation: accuracy, precision and DOP. Data relative to Paragraph 4.3.3

Point position	err_plane [m]	err_z [m]	sigma_plane [m]	sigma_space [m]	HDOP	PDOP
0-0 (Anchor 1)	0,043	-0,038	0,027	0,034	1,347	1,679
0-2	0,036	-0,133	0,025	0,059	1,230	2,956
0-4	0,033	-0,157	0,023	0,080	1,162	4,013
0-6	0,039	-0,111	0,023	0,078	1,159	3,892
0-8	0,047	-0,016	0,025	0,076	1,266	3,809
0-10	0,048	0,025	0,027	0,118	1,356	5,915
2-0	0,031	-0,160	0,023	0,058	1,153	2,888
2-2	0,026	-0,211	0,022	0,059	1,124	2,935
2-4	0,027	-0,219	0,021	0,059	1,061	2,966
2-6	0,038	-0,151	0,022	0,050	1,120	2,492
2-8 (Anchor 4)	0,050	-0,039	0,024	0,032	1,225	1,583
2-10	0,047	-0,021	0,025	0,076	1,269	3,810
4-0	0,022	-0,212	0,022	0,070	1,100	3,517
4-2	0,012	-0,256	0,020	0,063	1,005	3,137
4-4	0,015	-0,267	0,021	0,062	1,050	3,098
4-6	0,028	-0,224	0,021	0,055	1,045	2,750
4-8	0,038	-0,156	0,022	0,050	1,085	2,507
4-10	0,040	-0,114	0,023	0,074	1,164	3,694
6-0	0,028	-0,180	0,021	0,057	1,058	2,861
6-2	0,015	-0,240	0,021	0,062	1,039	3,115
6-4	0,001	-0,279	0,021	0,065	1,032	3,241
6-6	0,016	-0,263	0,021	0,066	1,060	3,299
6-8	0,026	-0,222	0,022	0,064	1,093	3,207
6-10	0,032	-0,166	0,024	0,080	1,196	3,998
8-0 (Anchor 2)	0,045	-0,037	0,025	0,031	1,235	1,566
8-2	0,025	-0,197	0,021	0,060	1,061	3,012
8-4	0,011	-0,268	0,022	0,076	1,082	3,778
8-6	0,015	-0,264	0,023	0,072	1,135	3,601
8-8	0,025	-0,213	0,024	0,058	1,179	2,884
8-10	0,033	-0,133	0,025	0,062	1,258	3,078
10-0	0,044	-0,028	0,028	0,137	1,406	6,851
10-2	0,032	-0,157	0,027	0,122	1,374	6,123
10-4	0,018	-0,237	0,027	0,107	1,343	5,358
10-6	0,021	-0,237	0,027	0,093	1,339	4,654
10-8	0,032	-0,157	0,027	0,064	1,358	3,219
10-10 (Anchor 3)	0,041	-0,038	0,030	0,036	1,490	1,792